Magnetic Resonance Spectroscopy in Metabolic and Molecular Imaging and Diagnosis of Cancer

Kristine Glunde,*[,†,‡] Dmitri Artemov,[†,‡] Marie-France Penet,[†] Michael A. Jacobs,[†,‡] and Zaver M. Bhujwalla*[,†,‡]

JHU ICMIC Program, Russell H. Morgan Department of Radiology and Radiological Science, and Sidney Kimmel Comprehensive Cancer Center, Johns Hopkins University School of Medicine, Baltimore, Maryland 21205

Received December 10, 2009

Contents

1. Introduction

Since its discovery in the 1940s, magnetic resonance spectroscopy (MRS) has developed into a major technique used by chemists to elucidate molecular structures. The underlying principle of MRS is the generation of radiofrequency (RF) signals by magnetic nuclear spins that are excited with a specific RF probe in an external magnetic field B_0. The magnetic resonance frequency ω_0 is linearly dependent on B_0 and the gyromagnetic ratio of the nucleus γ, as $\omega_0 = \gamma B_0$. The MR signal intensity depends on the concentration of nuclear spins, the magnetic field strength B_0, and the gyromagnetic ratio γ of these spins. The magnetization signal in MRS is characterized by two rate constants, the spin−lattice (or longitudinal relaxation time) T_1 and the spin−spin (or tranverse relaxation time) T_2. Since the resonance frequency of a particular nucleus is dependent upon its chemical environment, an important aspect of MRS is the ability to distinguish a nucleus with respect to its environment in the molecule. Because the molecular structure-based frequency shift and the resonance frequency are directly proportional to the strength of the magnetic field, the frequency shift is converted into a field-independent dimensionless value known as the chemical shift. Since the frequency shifts are extremely small in comparison to the resonance frequency, the chemical shift is expressed in parts per million (ppm). The chemical shift is typically reported relative to a reference resonance frequency. MRS therefore provides information about the chemical environment of the nuclear spin such as number of chemical bonds, neighboring nuclei, and overall chemical structure. As a result, each peak in an MR spectrum has a characteristic chemical shift that is dependent upon the chemical structure of the metabolite or compound and a peak area that is proportional to the concentration of the compound. Scalar spin−spin interactions, or J-couplings, produce fine multiplet structures that can be used to further analyze the chemical structure of a given molecule.

Within the past two decades, the same principles of chemical shifts, magnetic moments, relaxation rates, and deriving concentrations from peak integrals have been applied in several preclinical and clinical studies to advance cancer discovery, diagnosis, and treatment. Incorporating imaging techniques with MRS has resulted in the development of MR spectroscopic imaging (MRSI) where the chemical information is spatially phase encoded,[1−3] providing images of specific chemical compounds such as metabolites, reporter probes, labeled substrates, or drugs. The purpose of this article is to review recent developments and examples

Dr. Kristine Glunde is Associate Professor of Radiology and Oncology at the Johns Hopkins University School of Medicine. She received her Ph.D. from the University of Bremen in Germany in 2000. She was a Postdoctoral Fellow in the Molecular Cancer Imaging Program in the Department of Radiology at the Johns Hopkins University (JHU) School of Medicine. Since 2003, she has been a faculty member in the JHU *In Vivo* Cellular and Molecular Imaging Center (JHU ICMIC Program). Dr. Glunde's research focuses on developing novel optical imaging agents and techniques to study the role of lysosomal trafficking in breast and prostate cancer invasion and metastasis. She also studies mechanisms underlying the aberrant choline phospholipid metabolism in breast and prostate cancer using magnetic resonance spectroscopy and mass spectrometry imaging.

* To whom correspondence should be addressed. Kristine Glunde, Ph.D., Department of Radiology, Johns Hopkins University School of Medicine, 212 Traylor Bldg, 720 Rutland Ave, Baltimore, MD 21205. Telephone: (410) 614-2705. Fax: (410) 614-1948. E-mail: kglunde@mri.jhu.edu. Or Zaver M. Bhujwalla, Ph.D., Department of Radiology, Johns Hopkins University School of Medicine, 208C Traylor Bldg, 720 Rutland Ave, Baltimore, MD 21205. Telephone: (410) 955-9698. Fax: (410) 614-1948. E-mail: zaver@mri.jhu.edu.
† Russell H. Morgan Department of Radiology and Radiological Science.
‡ Sidney Kimmel Comprehensive Cancer Center.

10.1021/cr9004007
Published on Web 04/12/2010

Dr. Dmitri Artemov is Associate Professor of Radiology and Oncology at the Johns Hopkins University (JHU) School of Medicine. He received his Ph.D. from the Russian Academy of Sciences, Moscow. Before joining the JHU faculty, Dr. Artemov completed his postdoctoral training at the University of Wuerzburg and the Department of Radiology at the JHU School of Medicine. Dr. Artemov's research interests focus on developing novel molecular MR imaging methods to study tumors and on the role of stem cells in tumor progression and therapy.

Dr. Marie-France Penet is Instructor in the Molecular Cancer Imaging Program in the Department of Radiology at the Johns Hopkins University (JHU) School of Medicine. She received her Ph.D. degree from the University of Aix-Marseille in France in 2005. Dr. Penet's research focuses on using magnetic resonance imaging and spectroscopy together with histological and molecular analyses to understand the role of hypoxia and tumor vascularization and metabolism in prostate cancer invasion and metastasis.

Dr. Michael A. Jacobs is Associate Professor of Radiology and Oncology at the Johns Hopkins University (JHU) School of Medicine. His current research interests include developing radiological methods for detection, monitoring, and treatment of different pathologies, for example, using advanced MR methods for identification and classification of breast, prostate, and metastatic cancer, stroke, and uterine fibroids. He has pioneered the development of multiparametric analysis of different modalities to derive diagnostic biomarkers, as well as investigating the use of thermotherapy for treatment of tumors. Dr. Jacobs is on the National Board of the American College of Radiology Imaging Network (ACRIN) Breast Imaging committee and is the member of the subcommittee of molecular and functional imaging of the ACRIN. In addition, he is the Co-director of the Imaging Radiological Assessment Team (IRAT) at Johns Hopkins.

Dr. Zaver M. Bhujwalla is Professor in the Departments of Radiology and Oncology at the Johns Hopkins University (JHU) School of Medicine. She is the Director of the JHU *In Vivo* Cellular and Molecular Imaging Center. Dr. Bhujwalla joined the Department of Radiology at the Johns Hopkins University School of Medicine in 1989, just after completing her Ph.D. from the University of London. Dr. Bhujwalla's work has focused on the applications of MR imaging and spectroscopy and more recently multimodality imaging to understand and treat cancer. Dr. Bhujwalla is an elected Fellow of the International Society of Magnetic Resonance in Medicine and the American Institute of Biomedical Engineers. Dr. Bhujwalla is associated with the editorial boards of Molecular Imaging, NMR in Biomedicine, Cancer Biology and Therapy, and Contrast Media and Molecular Imaging.

of the use of multinuclear MRS in cancer and its integration with multimodality imaging in cancer discovery and treatment.

The ability of cancer cells to adapt and survive treatments, and the collateral damage to normal cells as a result of several cancer treatments, continue to make the successful treatment of cancer a major challenge for the 21st century. Tumor recurrence and metastasis are the leading causes of morbidity and mortality from cancer, and despite major advances in cancer research and treatment, cancer continues to evade cure. This is not surprising given the complexities of a tumor and the genomic plasticity of cancer cells and stromal cells that are co-opted within the tumor. A schematic of the different components of a tumor is shown in Figure 1.

Physiological conditions such as hypoxia and acidic extracellular pH (pHe) that exist in the tumor microenvironment, the interactions between cancer cells and stromal cells such as endothelial cells, fibroblasts, and macrophages, the extracellular matrix, and the numerous secreted factors and cytokines cumulatively influence progression, aggressiveness, and response of the disease to treatment. Hypoxia, in particular, is a major cause of radio- and chemoresistance in cancer cells. Because of the remarkable ability of cancer cells to adapt and survive, finding effective treatments against cancer depends upon identifying and attacking targets and pathways that are critically important for the cancer cell. Multinuclear MRS provides unique opportunities for molecular and functional imaging of cancer in preclinical and clinical studies, as well as for imaging interactions between cancer cells and stromal cells. Some of these applications of MRS, the nuclei commonly studied, and the information

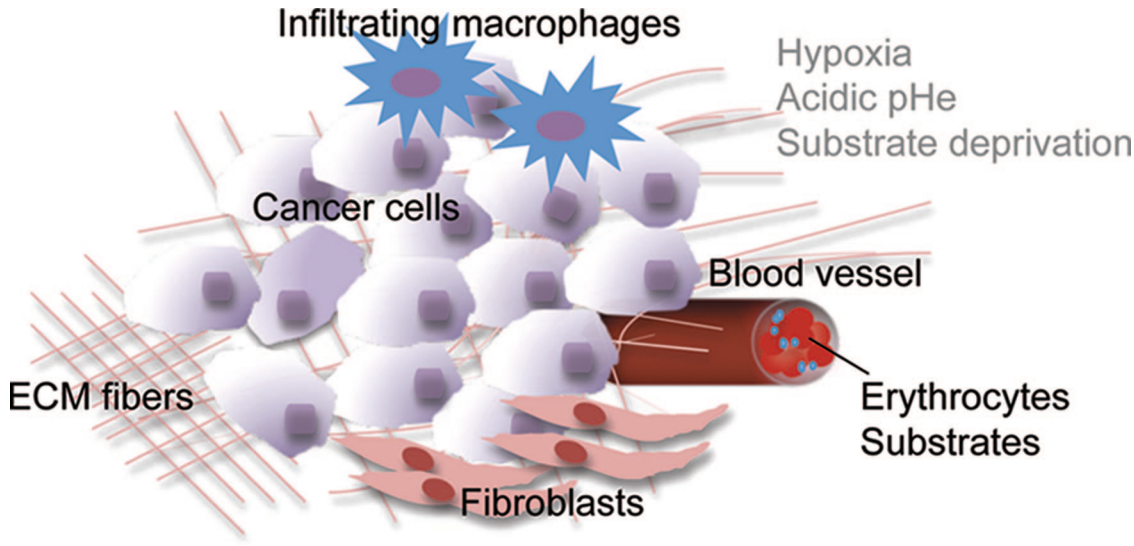

Figure 1. Schematic of the components of a tumor. Cancer cells are embedded within the extracellular matrix (ECM). The ECM consists of a complex meshwork of structural extracellular proteins. The tumor microenvironment (TME) contains the ECM and stromal cells such as endothelial cells, fibroblasts, and macrophages that are co-opted by the tumor. The TME is typically characterized by hypoxia, acidic extracellular pH (pHe), and substrate depletion.

Table 1. Nuclei Commonly Studied in Order of Sensitivity of Detection and Some of Their Preclinical (+) and Clinical (*) Applications in Cancer[a]

Nucleus	γ [MHz/T]	Sensitivity of detection	Applications
^{1}H	42.58		• Total choline+* • Lactate+* • Lipid+* • N-acetyl-aspartate+ • Citrate+ • Extracellular pH (pHe)+ • Treatment efficacy+* • Detection of metastasis+* • pO2+
^{19}F	40.08		• Drug pharmacokinetics+* • pHe+ • pO2+ • Enzyme activity+ • Labeled substrate utilization+
^{31}P	17.25		• Energy metabolism (ATP, PCr, Pi)+* • Intracellular pH (pHi)+* • Phospholipid metabolism+*
^{13}C	10.71		• Labeled substrate utilization to evaluate drug pharmacokinetics and metabolic pathways+*

[a] The intensity of the MR signal depends on the concentration of nuclear spins and the gyromagnetic ratio γ of the spins. The detection limits of ^{1}H and ^{19}F MRS are typically within the mM range, with higher concentrations required for less-sensitive nuclei such as ^{31}P and ^{13}C.

that can be obtained are summarized in Table 1. From this table, it is apparent that multinuclear noninvasive MRS methods have wide-ranging applications in cancer that can translate from bench to bedside. The chemical structures of various compounds referred to in this review article are summarized in Tables 2 and 3. Table 3 also provides details regarding administration and dose of the contrast agents described here.

The past decade has seen major advances in sequence design, development of novel reporter probes, and technological advances that have significantly increased the uses of MRS in molecular and functional imaging applications in oncology. Some of the recent applications of ^{1}H, ^{13}C, ^{31}P, and ^{19}F MRS in preclinical models of cancer are reviewed, and examples of biomedical MRS applications for each nucleus are shown in Figure 2. New developments, such as hyperpolarization of spins to increase the sensitivity of detection of the MR signal of ^{13}C-labeled substrates, are discussed. Advantages and limitations of the spectroscopic techniques and challenges for the future are outlined.

Table 2. Chemical Structures of Metabolites Referred to in This Review Article

Compound Name	Chemical Structure	Detected Nuclei	References
N-acetyl aspartate	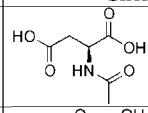	^{1}H	18-22
Citrate	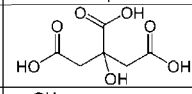	^{1}H	18-22
Glucose, [1-^{13}C]-/[U-^{13}C]-glucose	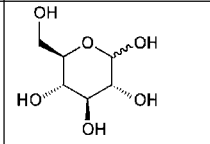 and/or 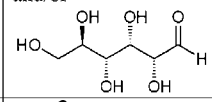	^{1}H, ^{13}C, hyperpolarized ^{13}C	15-18,63-68,71
Lactate, [3-^{13}C]-lactate, [1-^{13}C]-lactate	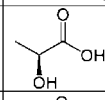	^{1}H, ^{13}C, hyperpolarized ^{13}C	15-18,63-68,71
[1-^{13}C]-pyruvate	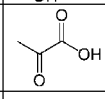	^{1}H, hyperpolarized ^{13}C	70,71,196
[1,4-$^{13}C_2$]-fumarate	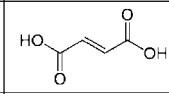	Hyperpolarized ^{13}C	70,196
Choline (Cho)	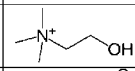	^{1}H	75-81
Phosphocholine (PC)	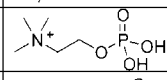	^{1}H, ^{31}P	75-81
Glycerophosphocholine (GPC)	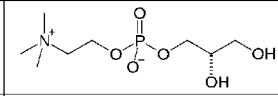	^{1}H, ^{31}P	75-82
Phosphoethanolamine (PE)	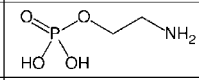	^{1}H, ^{31}P	82-84
Glycerophosphoethanolamine (GPE)	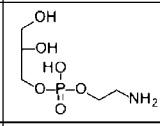	^{1}H, ^{31}P	82-84
Triacylglycerides, example of $C_{55}H_{98}O_6$, palmitic acid, oleic acid, alpha-linolenic acid (from top to bottom)	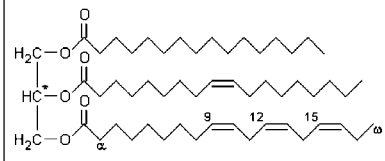	^{1}H	89-95
Nucleoside triphosphates (NTP), example of ATP	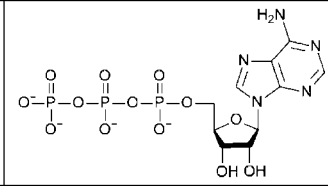	^{31}P	57,58,96-101
Nucleoside diphosphates (NDP), example of ADP	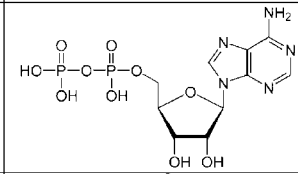	^{31}P	57,58,96-101
Phosphocreatine (PCr)	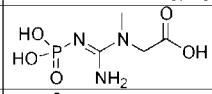	^{1}H, ^{31}P	57,58,96-101
Inorganic phosphate (Pi)	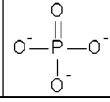	^{31}P	57,58,96-101

Table 3. Chemical Structures of Reporter Molecules Referred to in This Review Article

Compound Name	Chemical Structure	Detected Nuclei	Reported Property	Required Concentration	References
Hexamethyldisiloxane (HMDSO)	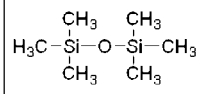	^{1}H	Oxygen Tension	Direct tissue injection of 50 μl pure HMDSO[11]	11,126
Hexafluorobenzene (HFB)	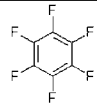	^{19}F	Oxygen Tension	Direct tissue injection of 40 μl pure HFB[125]	125,126
Nitroimidazoles, for example 2-Nitro-α-[(2,2,2-trifluoroethoxy)methyl]-imidazole-1-ethanol (TF-MISO)	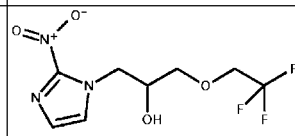	^{19}F	Oxygen Tension	75 mg/kg intravenous injection of TF-MISO (dissolved in saline)[129]	128-130
Inorganic phosphate (Pi)	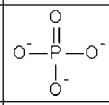	^{31}P, pH-dependent, chemical shift	pH, mostly pHi	Endogenous, ~1 mM	57,58,96-101
3-aminopropylphosphonate (3-APP)	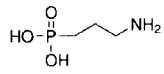	^{31}P	pHe	Intraperitoneal injection of 0.3 ml of 63.8 mg/ml 3-APP in saline[136]	136,207
2-imidazole-1-yl-ethoxy carbonyl propionic acid (IEPA)	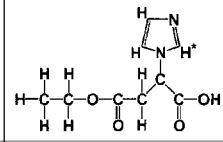	^{1}H	pHe	Intraperitoneal injection of 0.15 ml of 310 mM IEPA solution per 25 mg mouse[137,142,148]	137,142,148
Endogenous amide hydrogens in proteins		^{1}H CEST	Endogenous tissue pH, biodegradable molecular imaging reporter	~50 mM	112,113,149
Paramagnetic lanthanide chelates (ParaCEST), for example $EuCNPHC^{3+}$	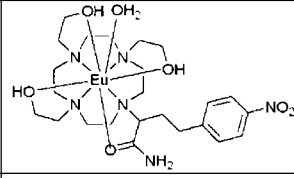	^{1}H ParaCEST	No *in vivo* studies available	~10 mM	150-153
Bicarbonate, ratio of $H^{13}CO_3^-$ to $^{13}CO_2$	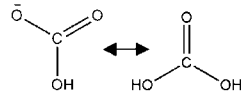	Hyper-polarized ^{13}C	Tissue pH	Catheter-based intravenous injection of 0.2 ml of 100 mM hyperpolarized $H^{13}CO_3^-$ solution[155]	155
[5-^{19}F]-fluorouracil (5-FU)	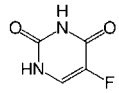	^{19}F	Drug Delivery and Metabolism of Chemotherapeutic Agent 5-FU	Humans are given a ~0.7 mM dose of [5-^{19}F]- FU[199]	199
[5-^{19}F]-fluorocytosine (5-FC)	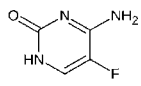	^{19}F	Pro-drug Therapy	Intraperitoneal injection of 5-FC at a dose of 450 mg/kg[201]	201
[^{13}C]-temozolomide (TMZ)	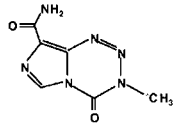	^{13}C	Drug Delivery of TMZ	Catheter-based intraperitoneal infusion of 0.3 ml of 3 mg/ml [^{13}C]TMZ in saline[204]	204

The use of MR biomarkers such as the total choline (tCho) signal and perfusion are already being explored clinically for characterizing tumors and following treatment response.[4−7] The elevation of choline compounds presents a unique target to exploit for molecular targeting; such targeting can be imaged noninvasively with MRS.[8,9] Both pharmacological and molecular approaches are being developed to target choline metabolism, specifically choline kinase activity, which is the first step in choline phospholipid biosynthesis.

The interaction between cancer cells and the tumor microenvironment is providing new insights into the etiology

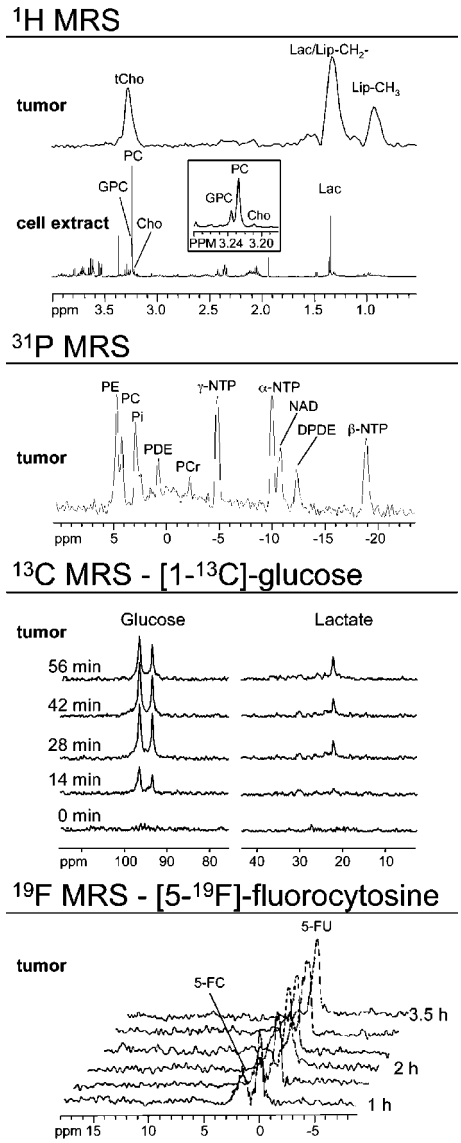

Figure 2. Examples of multinuclear MRS applications. From top to bottom: Representative in vivo single-voxel ^{1}H MRS of an MDA-MB-231 breast tumor xenograft model obtained at 4.7T, and ex vivo high-resolution ^{1}H MRS of a water-soluble MDA-MB-231 cell extract obtained at 11.7T.[17] The insert shows an expanded region around 3.2 ppm, demonstrating that human breast cancer cells exhibit low GPC levels, high PC levels, and high levels of total choline-containing metabolites. Representative in vivo single-voxel ^{31}P MRS of an MDA-MB-231 breast tumor model obtained at 4.7T.[191] Time course of in vivo ^{13}C MRS of a RIF-1 tumor obtained at 9.4T using heteronuclear cross-polarization.[52] The animal was injected with 900 mg/kg of [1-^{13}C]-labeled D-glucose. The glycolytic rate of the tumor can be determined by kinetic analysis of [3-^{13}C]-lactate build-up. Representative in vivo ^{19}F MRS of the conversion of prodrug to anticancer drug in an MDA-MB-231 breast tumor model.[201] The animal was injected with 450 mg/kg of [5-^{19}F]-fluorocytosine at 24 h after injection of a cytosine deaminase-containing nanoplex, and the conversion of the pro-drug [5-^{19}F]-fluorocytosine to the anticancer drug [5-^{19}F]-fluorouracil was followed by ^{19}F MRS at 4.7T. Assignments: Cho, free choline; 5-FC, [5-^{19}F]-fluorocytosine; 5-FU, [5-^{19}F]-fluorouracil; GPC, glycerophosphocholine; GPE, glycerophosphoethanolamine; NAD, nicotinamide adenine dinucleotide; DPDE, diphosphodiester; NDP, nucleoside diphosphate; NTP, nucleoside triphosphate; Lac, lactate; Lip-CH_2−, methylene groups of mobile lipids; Lip-CH_3, methyl groups of mobile lipids; PC, phosphocholine; PE, phosphoethanolamine; PCr, phosphocreatine; Pi, inorganic phosphate; tCho, total choline-containing compounds (Cho + PC + GPC). Adapted from refs 17, 52, 191, and 201.

and progression of cancer. For example, oxygen partial pressure (pO_2) in tumors can be imaged by both ^{1}H and ^{19}F MRSI.[10,11] Oxygen is sensed by administration of reporter molecules through changes in the spin−lattice relaxation rate. Integrating MRSI with MRI and other imaging modalities such as optical and nuclear imaging is providing useful insights into the dynamics between hypoxia and the tumor extracellular matrix (ECM), vascularization, extracellular pH, interstitial fluid transport, and metabolism in preclinical models.[12−14] These insights can be exploited to find effective treatment strategies.

2. Metabolic, Molecular, and Functional MRS of Cancer Cells and Their Microenvironment

2.1. Metabolic MRS

Along with, and frequently because of, aberrations in their genome and proteome, cancer cells exhibit a unique metabolic phenotype characterized by high glucose uptake, increased glycolytic activity and lactate production, decreased mitochondrial activity, low bioenergetic status, and aberrant phospholipid metabolism.[15−18] In addition, tissue-specific metabolites such as *N*-acetyl aspartate in the brain, and citrate in the prostate, decrease as the cancer cell population in the tissue expands.[18−22] The chemical structures of glucose, lactate, *N*-acetyl aspartate, and citrate are shown in Table 2. MRS or MRSI detection of the ^{1}H or ^{31}P MRS signals of these endogenous metabolites can assist in the diagnosis of cancer[23−46] and in monitoring anticancer therapy in cases where these metabolites have been established as surrogate markers for a specific therapy, as discussed in section 3.2. Detection of aberrant metabolism with MRS can also lead to the identification of enzymes as novel anticancer targets.[9,17,47−51]

Labeled Substrates

In addition to the detection of endogenous metabolites using ^{1}H or ^{31}P MRS, ^{13}C MRS detection of ^{13}C-labeled metabolites can be performed following administration of suitable ^{13}C-labeled substrates in cancer cells and solid tumors to study glycolysis (see Figure 2) or other metabolic pathways such as choline metabolism.[8] The flux of substrates through metabolic pathways can be evaluated by detecting the incorporation of ^{13}C label into downstream metabolites and products with ^{13}C MRS, followed by metabolic modeling. The relatively low sensitivity of ^{13}C MRS can be improved by a number of magnetization transfer techniques such as nuclear Overhauser effect (NOE), heteronuclear cross-polarization (HCP) experiments,[52] and indirect inverse detection methods.[53] Such methods enable detecting ^{13}C label with sensitivity close to that of ^{1}H MRS, which significantly increases the detection sensitivity of ^{13}C-labeled metabolites in vivo. Weak ^{13}C signals are enhanced by transferring strong magnetization from the neighboring protons via space using dipole−dipole spin coupling (in NOE methods) or through chemical bonds via J-coupling between ^{13}C and ^{1}H spins. In direct detection methods such as NOE, distortionless enhancement by polarization transfer (DEPT), insensitive nuclei enhanced by polarization transfer (INEPT), and HCP, the enhanced ^{13}C signals are detected directly with broadband proton decoupling. In the indirect detection scheme, the magnetization is transferred from ^{1}H to ^{13}C and then back to protons in heteronuclear multiple quantum coherence

(HMQC) and heteronuclear single quantum coherence (HSQC) methods. The ^{13}C signals are thus detected indirectly as ^{1}H frequencies with significantly enhanced sensitivity due to the higher gyromagnetic ratio γ of ^{1}H.[53]

Glucose/Lactate

Cancer cells exhibit high glycolytic activity even in the presence of oxygen,[54,55] an observation made by Otto Warburg in 1930 and subsequently called the "Warburg effect". The molecular mechanisms underlying this aerobic glycolysis are mediated, in part, through the stabilization of the hypoxia inducible factor alpha (HIF-1α).[55] HIF-1α expression mediates a switch in glucose metabolism through the induction of lactate dehydrogenase, which converts pyruvate to lactate, and by the inactivation of pyruvate dehydrogenase, the enzyme responsible for the conversion of pyruvate to acetyl−Coenzyme A.[56] The poor blood flow in tumors and the resulting hypoxia also contribute toward increasing anaerobic glycolysis.[57,58] Glucose uptake within cells also increases through up-regulation of glucose transporter GLUT-1 and -3 expression, and possibly other GLUTs.[59,60] As a result, cancer cells rapidly metabolize glucose to form lactate. Intravenous infusion of [1-^{13}C]-labeled glucose enables the investigation of glycolysis in vivo and detection of the kinetics of [3-^{13}C]-labeled lactate formation, as shown in the ^{13}C MR spectra in Figure 2. Glucose uptake, delivery, and glycolytic breakdown, as well as lactate synthesis and clearance from the tumor, can be derived by following the ^{13}C-label of these substrates.[61] Several factors, such as tumor hemodynamics, substrate supply, hypoxia, venous clearance, glucose supply, extent of necrosis, and degree of inflammatory cell infiltrate, contribute to lactate levels in tumors.[62] Multiple signaling pathways and oncogenes can regulate glycolysis.[54] Decreasing tumor oxygenation correlated with increasing glycolytic rate in a murine mammary carcinoma model in a study using volume-localized ^{13}C MRS with $^{1}H-^{13}C$ cross-polarization to detect the conversion of [1-^{13}C]-glucose to [3-^{13}C]-lactate.[63] Several studies showed that [1-^{13}C]-labeled glucose is metabolized to lactate in poorly differentiated tumors.[64−67] High-resolution (HR) ^{13}C MRS studies of tumor or organ extracts from animals infused with [1-^{13}C]- or [U-^{13}C]-labeled glucose reveal complex ^{13}C-labeling patterns of various metabolites that can provide insight into metabolic compartmentalization, shuttling of metabolites between cell types or organs, and metabolic fluxes.[68] See Table 2 for the chemical structures of glucose, pyruvate, and lactate.

Hyperpolarization

The large increase of sensitivity introduced by the use of dynamic nuclear polarization (DNP) for solution-state magnetic resonance spectroscopy (DNP-MRS)[69] for in vivo MRS and MRSI detection of hyperpolarized ^{13}C-labeled substrates has revitalized ^{13}C MRS studies.[70,71] Theoretically, DNP can increase the detection sensitivity of hyperpolarized ^{13}C-labeled substrates and their metabolites by as much as 10 000-fold, without background signal from nonpolarized material.[70,71] DNP is based on polarizing nuclear spins in the solid state.[72] The mechanism requires the availability of unpaired electrons, which are added to the sample as homogeneously distributed organic free radicals before cooling the sample.[69] In the solid state, the high electron spin polarization is, in part, transferred to the nuclear spins by microwave irradiation and subsequently brought into a liquid solution after rapid dissolution.[69] With this method, it is possible to bring the polarized, cold, solid sample into solution while preserving its nuclear polarization for a short time, sufficient for spectroscopic imaging.[69] However, complexities in terms of the physical chemistry of achieving hyperpolarization in the solid state, the appropriate free radicals, and the limited number of molecules amenable reduce the achievable sensitivity. Commercial DNP-MR spectrometers and hyperpolarizers are currently becoming available. Elevated hyperpolarized lactate and possibly alanine produced from hyperpolarized [1-^{13}C]-labeled pyruvate are being actively investigated as noninvasive biomarkers of cancer presence and histologic grade in preclinical models, which may be used in the future for the detection and management of cancer in humans.[71] An alternative mechanism to hyperpolarize ^{13}C nuclei includes the use of parahydrogen to hydrogenate multiple bonds in chemical structures containing enriched ^{13}C isotopes (PASADENA).[73,74] Parahydrogen based hyperpolarization requires ^{13}C substrates with a specific chemical structure, which may limit its general applicability in comparison to DNP-based methods.

Choline Phospholipid Metabolism

Choline phospholipid metabolism is significantly altered in cancers, as validated by several preclinical and clinical studies.[75−79] Almost all cancers display elevated phosphocholine (PC) and increased total choline-containing metabolites (total choline, tCho).[75−79] A switch from high glycerophosphocholine (GPC)/low PC to low GPC/high PC can be detected following malignant transformation in breast[80] and ovarian[81] cancer cells by HR ^{1}H or ^{31}P MRS of cell extracts (see ^{1}H MRS of cell extract in Figure 2). These metabolic changes can be detected in vivo and in biopsied tumor tissue ex vivo by ^{1}H or ^{31}P MRS of the endogenous metabolites. The predominant ^{1}H MRS signals from water-soluble choline metabolism intermediates arise from the nine chemically equivalent protons in the choline $-N(CH_3)_3$ groups between 3.2 and 3.3 ppm. Because nine protons contribute to the signal, it displays a relatively higher signal intensity than ^{1}H signals detected in chemical groups with fewer equivalent protons. Free choline (Cho) is typically detected at 3.21 ppm, PC at 3.23 ppm, and GPC at 3.24 ppm, measured at pH 7.4 with 3-(trimethylsilyl)propionic-2,2,3,3-d_4 acid as a chemical shift reference, in HR MR spectra of cell or tissue extracts, or in HR magic angle spinning (MAS) MR spectra of biopsies. In the in vivo setting, the spectral resolution that can be achieved even at high magnetic fields is much lower and unable to resolve Cho, PC, and GPC, as evident in the ^{1}H MR spectra in Figure 2. Instead, an overlap of these three signals is detected as the tCho signal. The chemical structures of Cho, PC, and GPC are shown in Table 2.

Currently, clinical multicenter trials are underway to establish ^{1}H MRS of a single voxel covering a region of interest, such as, for example, a lesion for breast cancer detection. Single-voxel ^{1}H MRS detects a single localized MR spectrum. Alternatively, in vivo ^{1}H MRS imaging (MRSI) can be performed of one or multiple slice(s) through a region of interest. Multi-voxel techniques, in which multiple spectra are acquired over a slice or volume of tissue, enabling the detection of the spatial distribution of tCho (as well as other metabolites), are being developed. Such two-dimensional or three-dimensional MRSI have been used to detect

elevated tCho in vivo in several types of cancer as discussed in section 3. The ^{31}P-containing choline metabolites can also be detected with ^{31}P MRS, as shown in Figure 2. HR ^{31}P MR spectra of extracts detect PC at 3.9 ppm and GPC at 0.5 ppm, upon chemical shift calibration to a reference compound, such as methylene diphosphonic acid at 18 ppm. Phosphorus MRS in vivo detects a mixed phosphomonoester (PME) signal comprising unresolved PC and phosphoethanolamine (PE) resonances, and a mixed phosphodiester (PDE) signal comprising unresolved GPC and glycerophosphoethanolamine (GPE) resonances. PC and PE, and/or GPE and GPC, can be partially resolved in clinical studies by using ^{1}H-decoupled ^{31}P MRS techniques at 1.5T,[82] as well as at higher field strengths that are clinically available, such as 3T. However, in vivo clinical studies often favor ^{1}H MRS because of its higher sensitivity and better availability on clinical scanners when compared to ^{31}P MRS. Neither ^{1}H nor ^{31}P MRS in routine in vivo settings are able to spectrally resolve Cho, GPC, and PC as individual signals. As a consequence, noninvasively detected PME, PDE, and tCho changes in in vivo ^{31}P and ^{1}H MR spectra often arise from changes in the concentrations of several different metabolites. In some cases, this can be overcome by acquiring consecutive proton-decoupled ^{31}P and ^{1}H MR spectra.[83] Recently, a novel ^{1}H to ^{31}P polarization transfer method was developed on a clinical 3T MR scanner, which improved the signal-to-noise ratio by more than 2-fold compared to direct ^{31}P MRS methods.[84] This method achieved ^{1}H to ^{31}P polarization transfer by applying chemical shift selective refocusing pulses at 3T, which canceled the homonuclear J-coupling effects that attenuate ^{31}P signals in PE, PC, GPE, and GPC in previous refocused INEPT experiments.[84] The method allowed the identification of these four metabolites in human brains with a voxel size of $2 \times 2 \times 2$ cm^3 in a three-dimensional MRSI data set.[84] The chemical structures of these metabolites are shown in Table 2.

The increased PC levels observed in cancer cells and tumors result from increased expression and activity of choline kinase,[48−50] a higher rate of choline transport,[85,86] and increased phospholipase C and D activity.[81,87] These enzymes, among others, are involved in the biosynthetic and breakdown pathways of the major membrane phospholipid phosphatidylcholine (PtdCho), the precursors and breakdown products of which are GPC, PC, and Cho.[8] Some of these enzymes, such as choline kinase[9,17,47−51] and PtdCho-specific phospholipase D[88] and C,[81] have recently been developed for MRS-monitored, targeted anticancer therapies, mediated by gene silencing or enzyme inhibition, as discussed in detail in section 3.2. Enzymes in choline phospholipid metabolism are influenced by growth factor signaling, cytokine action, oncogene activation, and chemical carcinogenesis.[17,75,76] The chemical structures of choline- and ethanolamine-related compounds are shown in Table 2.

Mobile Lipids

In vivo single-voxel ^{1}H MRS and MRSI detect several signals that are related to choline and lipid metabolism, such as the total choline (tCho) signal at 3.2 ppm, the methylene signal at 1.3 ppm, and the methyl signal at 0.9 ppm (see representative ^{1}H MR spectra in Figure 2). These methylene and methyl signals arise from CH_2 and CH_3 groups in mobile lipids located in the cytoplasm of intact cancer cells, or in the intercellular space of solid tumors.[89,90] The lipid signals at 1.3 and 0.9 ppm detected in intact cells and tumors in vivo have been assigned to the fatty acid acyl chains in triacylglycerides (see Table 2 for chemical structure) that form mobile lipid droplets.[89,90] The low mobility of membrane lipids limits their detection by MRS in vivo, and therefore, membrane lipids do not contribute to these lipid signals at 1.3 and 0.9 ppm.[89,90] These lipid signals overlap with various other signals, such as lactate at 1.3 ppm, and spectral editing is required to separate these signals. Additional signals at 5.4 and 2.8 ppm can be assigned to mobile polyunsaturated fatty acyl chains to assess polyunsaturation of mobile lipids,[90] although the signal at 5.4 ppm is difficult to detect because of its proximity to the large water signal at 4.7 ppm. High-grade human gliomas displayed significantly higher levels of lipid than low-grade gliomas, suggesting that the lipid signal at 1.3 ppm may prove useful in tumor grading.[89] Lipid droplets in tumors were also shown to correlate with drug resistance or response.[89] The cytoplasmic accumulation of triacylglycerides in cancer cells and tumors has been attributed to such diverse biological processes as hypoxia, degeneration of mitochondria, differentiation, growth arrest, and apoptotic cell death.[89−91] Triacylglycerides are formed from increased diacylglycerol and triacylglycerol biosynthesis in lipid metabolism.[90,91] Changes in the mobile lipid signal have also been observed following apoptosis, necrosis, or lipid droplet formation.[92−94] MRS-visible lipids accumulate with apoptosis,[95] suggesting that this signal may serve as a surrogate marker for apoptosis, detected in vivo by ^{1}H MRS.

Energy Metabolism

While ^{31}P MRS is useful for detecting energy metabolism in vivo,[96−99] it suffers from poor sensitivity, and therefore, its use has declined in recent years, especially for clinical studies. Solid tumors contain nucleoside triphosphates (NTP), nucleoside diphosphates (NDP), phosphocreatine (PCr), and inorganic phosphate (Pi), all of which can be detected in ^{31}P MR spectra (see Figure 2). The chemical shift of the Pi resonance can be used to calculate the pH of the tumor as outlined in section 2.3. Because of the Warburg effect, the bioenergetic state of cancer cells is relatively low.[54] Since the production of high-energy phosphates such as NTP and PCr depends on glucose and oxygen, which are delivered to tumors through blood vessels, energy metabolism is tightly coupled to tumor blood flow[100,101] and decreases in hypoxic regions. Vaupel et al.[57,58] observed a significant positive correlation between the ^{31}P MRS-detected ratios of PCr/Pi and NTP/Pi with tumor oxygenation. In preclinical studies, ^{31}P MRS may be useful in detecting blood flow mediated changes in tumor reoxygenation[102] during radiation therapy.[103] The chemical structures of high-energy phosphates are shown in Table 2.

HR-MAS MRS

High-resolution magic angle spinning (HR MAS) ^{1}H MRS is a relatively new technology for examining intact biological tissue ex vivo, such as biopsy specimens, at high spectral resolution.[22,104−109] One of the advantages of HR MAS ^{1}H MRS, in comparison to HR MRS of extracts, is that the tissue can be used subsequently for histologic, biochemical, and genetic analysis.[22,104−109] HR MAS ^{31}P MRS is sensitive enough to be a potential future tool for assessing phospholipid metabolism in tumor samples prior to histopathologic examination.[110]

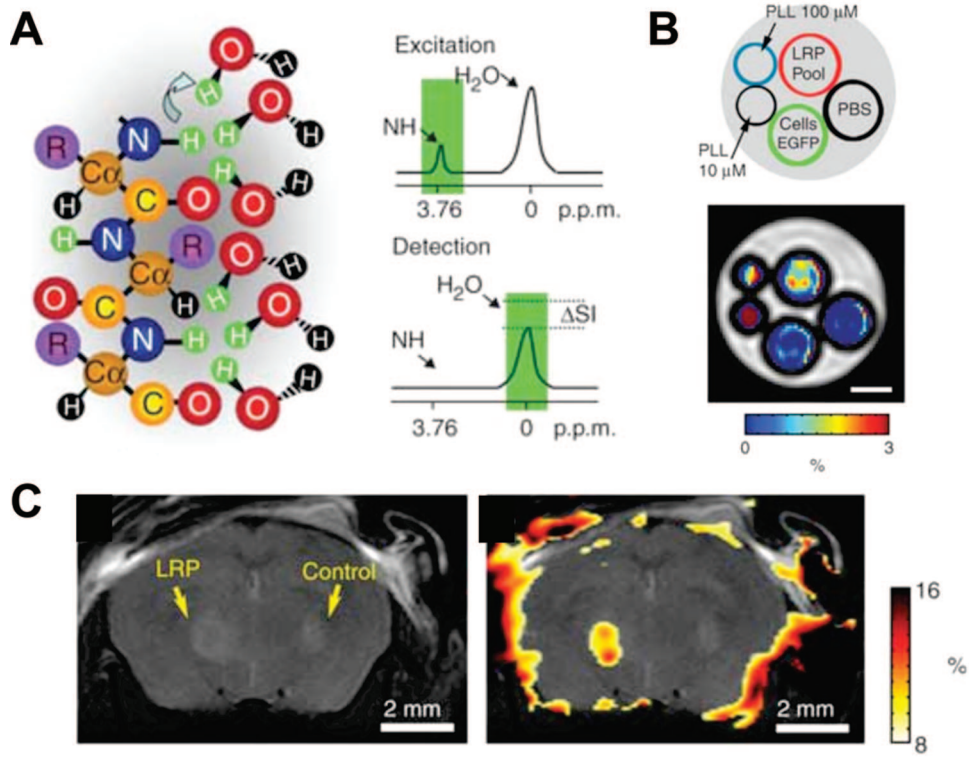

Figure 3. CEST imaging of lysine rich-protein (LRP) reporter. (A) Frequency-selective radiofrequency pulses excite the amide protons. These protons exchange with water protons, thereby reducing the MRSI signal intensity (SI) of the water signal by ΔSI. (B) Ex vivo proof-of-principle MRSI of the LRP reporter protein in phantoms demonstrated that the LRP-containing phantom displayed significantly higher ΔSI when excited at ±3.76 ppm as compared to poly-L-lysine, phosphate-buffered saline, or green fluorescent protein as controls (scale bar, 1 mm). (C) Anatomical image (left) and CEST signal intensity-difference map overlaid on the anatomical image (right) was able to distinguish the LRP-expressing and control tumor xenografts. Adapted from ref 114.

2.2. Molecular MRS

Magnetization transfer (MT) is a frequency-selective MR technique that can be employed to evaluate ^{1}H and other nuclei chemical exchange to study chemical reactions.[111] Proton chemical-exchange-dependent saturation transfer (CEST) can provide, among other applications, a strategy to measure pH in vivo as outlined in section 2.3. Exogenous CEST-contrast agents have been tested, demonstrating the feasibility of detecting a CEST-based MRI contrast agent.[112] Detecting amide protons of endogenous mobile cellular proteins and peptides (see Table 3 for chemical structure, chemical shift of 8.3 ± 0.5 ppm) that undergo proton exchange with water has been demonstrated by ^{1}H MRS and MRI.[113] Amide proton CEST contrast was achieved by selectively irradiating amide protons with a radiofrequency pulse at 8.3 ppm; water was imaged after several seconds of transfer, and the MT ratio asymmetry parameter was calculated.[113] Recently, a novel nonmetallic, biodegradable, lysine rich-protein (LRP) reporter was genetically engineered to provide a CEST reporter protein with frequency-selective contrast,[114] as demonstrated in Figure 3. Similar to fluorescent proteins in optical imaging, such CEST reporter proteins can be used for molecular imaging studies in gene promoter or gene expression studies, in which ^{1}H MRI is used as the imaging modality. Figure 3A shows the principle of CEST. Frequency-selective radiofrequency pulses saturate the excitation of amide protons in LRP, which exchange with water protons and decrease the detected signal intensity (SI) of the water signal. Figure 3B and 3C shows that ex vivo and in vivo LRP reporter imaging is feasible. To date, several different polypeptides have been tested for their feasibility as "multicolor" CEST reporters.[115] These different CEST reporter proteins can be assigned artificial colors based on their particular amino acid units (lysine, arginine, threonine, or serine), which lead to different resonance frequencies of the exchangeable protons in different CEST reporters.[115] These new CEST agents are potentially suitable for designing MR reporter genes for cell and tumor imaging, as well as for distinguishing multiple targets within the same MR image.[115]

2.3. Tumor Microenvironment—Hypoxia and pH

The tumor microenvironment is usually characterized by areas of hypoxia, a neutral to alkaline intracellular pH (pHi), and an acidic extracellular pH (pHe).[57] Hypoxia arises in tumors from the chaotic and abnormal vasculature that results in areas with poor oxygenation and substrate supply.[116] If the hypoxia is severe enough, these areas will ultimately progress to form necrosis. pHi depends upon the buffering capacity of the cell, the efficiency of proton pumps in the plasma membrane, and the rate of proton production.[117] Extracellular pH also depends upon these factors, and additionally, on the ability of the vasculature to clear the protons.[117] Both hypoxia and an acidic pHe result in a more aggressive phenotype,[118] and hypoxia results in radiation- and chemoresistance.[119] MRS reporters that noninvasively measure pH and oxygen tension are therefore useful for selecting treatments and following changes in these parameters during treatment. Since these parameters are spatially heterogeneous, techniques that provide spatial information are the most useful. Global unlocalized information, however, is also valuable for understanding cancer pathophysiology

and for developing effective therapeutic strategies that target hypoxia and pH.

Imaging Hypoxia by MRS/I

Perfluorocarbons (PFCs) have been used as probes to measure pO_2 using ^{19}F MRS because their relaxivity is strongly dependent on the concentration of dissolved molecular oxygen.[120−123] The advantages of ^{19}F MRS-based oxygen probes are a relatively high sensitivity due to the large gyromagnetic ratio of the ^{19}F nucleus and the absence of endogenous ^{19}F-containing molecules in the body. More recently, an analogous approach with ^{1}H MRS has been developed using hexamethyldisiloxane (HMDSO).[11] Proton MRS has the highest sensitivity, but it is important that the reporter signal has a chemical shift that is well-separated from metabolite signals and the water signal to avoid overlap. HMDSO has a single signal close to that of tetramethysilane and is, therefore, well-separated from metabolites and water. Ideally, these reporters should also have a single resonance, have a low temperature sensitivity, and display a linear response to pO_2. PFCs and HMDSO are poorly water-soluble and, therefore, have to be administered as an emulsion. Intravenous administration of PFC emulsion results in uptake by the reticuloendothelial system and the localization of the probe in the tumor periphery, which may skew measurements toward well-perfused regions.[124−126] Alternatively, similar to the use of an Eppendorf electrode, the probes can be injected directly into the tissue to report on oxygen tensions in regions of interest, with the advantage of being able to follow oxygenation over a period of time.[127] Both ^{1}H MRS-detected HMDSO and the symmetric ^{19}F MRS-detected PFC hexafluorobenzene (HFB) have a single resonance and a temperature-insensitive, oxygen-dependent relaxivity.[126] Both probes have previously been used to measure oxygen tensions in tumor models.[126] The high sensitivities of ^{19}F and ^{1}H allow spatial localization for detection of these probes with an in-plane resolution of ~1 mm. The temporal resolution, which depends upon the ability to detect adequate signal at physiological nontoxic concentrations, is typically on the order of an hour or less. To date, these probes have not been used clinically.[126] The chemical structures of HMDSO and HFB are shown in Table 3.

Qualitative measurements of tumor hypoxia have also been performed using ^{19}F MRS of reporter molecules such as nitroimidazoles, which accumulate in hypoxic cells.[128,129] Nitroimidazoles are reduced by one-electron nitroreductase enzymes under hypoxic conditions to form reduction products that bind to endogenous cellular molecules. In the activation reaction, the addition of the first electron to form a nitro-radical anion is reversible in the presence of oxygen. Therefore, the process is dependent on oxygen concentration, and an accumulation of these reporters can be used to estimate hypoxia.[130] A potential problem is that two-electron reductases such as DT-diaphorase ([NAD(P)H:(quinone-acceptor) oxidoreductase], EC 1.6.99.2) can reduce nitroimidazoles in two-electron steps, resulting in the reduction occurring independently of oxygen concentration.[131,132] In addition, the adducts formed are short-lived.[132]

Imaging Tumor pH by MRS/I

In 1973, Moon and Richards observed that the chemical shift of intracellular phosphates in whole blood was sensitive to pH.[133] This led to the development and use of the Pi peak to measure pH with MRS. Both intra- and extracellular Pi contribute to the Pi signal in vivo (see Table 3 for chemical structure). In tumors, the Pi signal is primarily of intracellular origin.[134] As a result, the chemical shift of Pi reports on intracellular pH (pHi). Since tumors are highly glycolytic, the concept of an acidic tumor pH had become commonly accepted until ^{31}P MRS of tumors demonstrated that tumor intracellular pH was typically neutral or alkaline.[135] The subsequent development of an extracellular pH probe, 3-aminopropylphosphonate, 3-APP (for chemical structure see Table 3),[136,137] allowed simultaneous detection of intra- and extracellular pH in tumors. These studies further confirmed that the extracellular pH (pHe) of tumors is acidic, while the intracellular pH (pHi) is neutral-to-alkaline. Acidic pHe has been observed to stimulate invasion in culture.[138] pH can be increased in vivo by chronic or acute treatment with bicarbonate.[139] Interestingly, a recent study has shown that mice treated with bicarbonate developed significantly fewer metastases.[140] Phosphorus MRS has been used to measure pHi in human cancers,[75] but as yet probes to measure pHe in humans are not available. Other than acquiring spectra from 3−4 mm thick tumor slices or using large voxel sizes of $\sim 6 \times 6 \times 6$ mm^3 localized on the tumor to avoid including signals from normal tissue, the low sensitivity of ^{31}P MRS does not allow acquisition of spectra with high spatial resolution.

Several pH-sensitive probes for ^{1}H and ^{19}F MRS[141−144] have been used to measure localized tumor pH using MRSI with spatial resolutions approaching $1 \times 1 \times 1$ mm^3.[137,142,145,146] These pH probes are based on imidazole compounds.[141,146,147] One imidazole-based compound, 2-imidazole-1-yl-ethoxy carbonyl propionic acid (IEPA, for chemical structure see Table 3), has been used to image tumor pHe in several tumor models. Consistent with earlier findings, the probe reported an acidic and heterogeneous pHe.[137,142,148] IEPA has also been used in combination with vascular MRI to obtain colocalized multiparametric data sets.[142] By combining MRSI of pHe with vascular MRI measurements, it is possible to exploit the multiparametric capability of MR to understand the dynamics between pHe and vascular parameters in tumors with different phenotypic characteristics.[142]

Chemical exchange saturation transfer (CEST) has also been used to measure pH by determining the rate of acid-catalyzed exchange of exogenous or endogenous amide hydrogens with bulk water.[112,113,149] CEST is relatively insensitive, requiring more than a 50 mM concentration of exchangeable amides (chemical structure shown in Table 3). Although the sensitivity of detection can be improved by using pH-sensitive paramagnetic lanthanide chelates (ParaCEST, see Table 3 for the chemical structure of a representative example),[150−152] this approach still requires ~10 mM contrast agent and is also concentration-dependent. Therefore, it is necessary to determine the concentration of the probe.[153] A recent approach of attaching a ^{19}F-moiety on the same carrier as the pH-responsive paramagnetic complex provides a strategy to normalize the concentration of the probe.[154]

One exciting development in the use of MRS to measure tumor pHe is the application of hyperpolarized ^{13}C-labeled bicarbonate (see Table 3 for structure).[155] This nontoxic probe, which can be infused in humans at relatively high concentrations, utilizes the cellular buffering systems to determine pHe. By DNP of ^{13}C-bicarbonate, the sensitivity of ^{13}C detection is increased by as much as 10 000-fold, which allows for ^{13}C MRSI of tissues in vivo. The ratio of

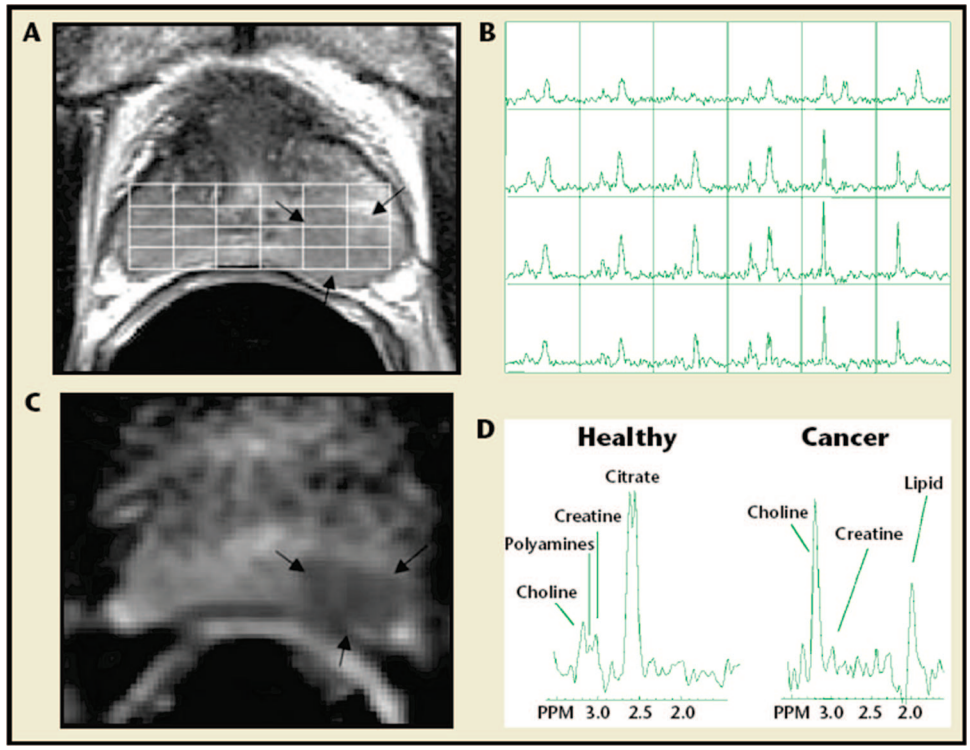

Figure 4. Combined MRI, DWI/ADC mapping, and MRSI of the prostate at 1.5T. (A) Axial T_2-weighted image and three-dimensional MRSI spectral grid. The arrows indicate a region of prostate cancer. (B) Corresponding MRSI spectral array, showing the presence of an aggressive tumor (elevated total choline and reduced citrate) on the left side of the gland (right side of the image). (C) Image of the apparent diffusion coefficient of water demonstrates a region of prostate cancer (arrows) in the same location as the T_2-weighted image and MRSI. (D) Representative spectra taken from the region of healthy prostate tissue (left) and prostate cancer (right). Adapted from ref 170.

$H^{13}CO_3^-$ to $^{13}CO_2$ is used to determine pH, assuming a pK_a of 6.17. Initial preclinical studies demonstrated the feasibility of obtaining pHe maps with a spatial resolution of $2 \times 2 \times 6$ mm^3. The availability of such a nontoxic probe may be used, in the future, to image pH in humans not only in oncology but also in other disease processes with abnormal acid−base conditions.

3. MRS Applications in Diagnosis and Therapy Monitoring

3.1. Diagnosis

In vivo ^{1}H MRS provides clinically useful information and is routinely implemented in the majority of clinical MR scanners.[23,37,42,156−159] In addition to standard dynamic contrast-enhanced (DCE) MR imaging (MRI), quantitative ^{1}H MRS and ^{1}H MRSI measurements of tCho, in addition to other tissue-specific metabolites, are increasingly being implemented to diagnose primary malignant tumors in brain,[23−34] prostate,[35−38] and breast.[39−46,160] The addition of MRS to standard MRI techniques can lead to significant improvements in sensitivity of up to 88%, specificity of greater than 90%, and diagnostic accuracy of up to 91%. Choline phospholipid metabolism intermediates, among other metabolites, can also serve as robust biomarkers ex vivo, when analyzed in human biopsy specimens using HR ^{1}H MRS or HR MAS ^{1}H MRS. High tCho and PC concentrations have been used to identify meningiomas and recurrent astrocytomas in human brain tissue specimens,[161] breast cancer in fine-needle aspirates of breast tumors,[162] prostatic carcinoma in postsurgical prostate tissue samples,[21] and well-differentiated liposarcomas in surgically resected fat tissue specimens.[20]

As discussed in detail in section 2.1, significant spectral differences exist between normal tissue and tumors. One of the most reliable differences is observed in tCho, with low tCho concentration in normal tissue and high tCho levels in tumors.[23,42,158,159] Proton MRS and MRSI can therefore be used clinically to help diagnose cancer and to determine the margins of brain,[23−25,163] prostate,[158,159] and breast[5,40−42,164,165] tumors, among others. Clinical ^{1}H MRS detection of tCho can also help differentiate tumor recurrence from necrosis following antitumor treatment in brain[166−168] or prostate.[169] As single-voxel ^{1}H MRS or MRSI detects changes in tCho and other metabolites such as creatine, *N*-acetyl-aspartate (NAA), and lactate (see Table 2), obtaining metabolite ratios can improve the specificity of detection. Figure 4 shows an example of multiparametric MR of the prostate, which includes an apparent diffusion coefficient (ADC) map from diffusion-weighted imaging (DWI), and three-dimensional MRSI acquired at 1.5T. The three-dimensional MRSI spectral array in Figure 4B shows the presence of an aggressive tumor that contains elevated tCho and reduced citrate on the left side of the gland (right side of the image).[170]

In current radiological practice, several MRI parameters, such as T_2-weighted contrast, T_1-weighted DCE-MRI, and DWI are combined to identify suspicious lesions in the prostate. Normal prostatic tissue has high T_2-weighted MRI signal, whereas low T_2-weighted MRI signal was found to correlate with pathological prostatic tissue.[171] Studies at 3T have demonstrated an increase in sensitivity

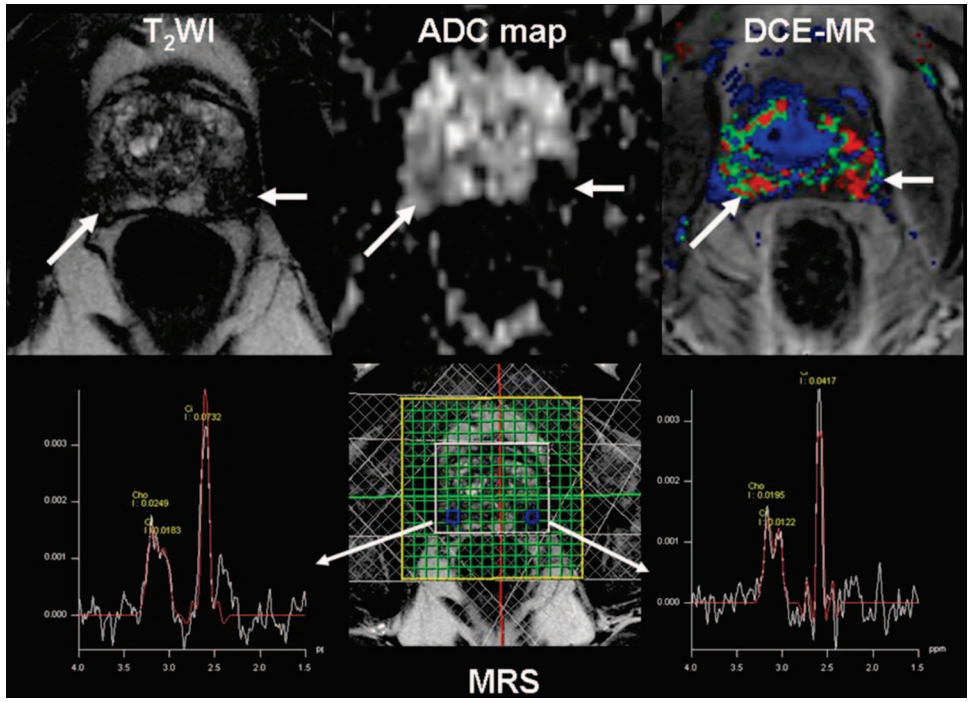

Figure 5. Demonstration of T_2-weighted image, DWI/ADC map, MRS, and DCE-MRI of a 55 year old man with suspected prostate cancer (Gleason score = 7). Multiparametric MRI of the prostate gland revealed focal areas of "dark" T_2 signal bilaterally with corresponding decreased ADC in the left/mid area of the gland ($0.41 \pm 0.13 \times 10^{-3}$ mm^2/s) and $0.97 \pm 0.34 \times 10^{-3}$ mm^2/s on the right side (although a smaller region). DCE-MRI kinetics detect increased permeability and extravascular fraction in the right and left mid-gland areas that are correlated to the Gleason score of 7. Moreover, both sides show evidence of increased total choline and decreased citrate by MRS. Adapted from ref 172.

and specificity using T_2-weighted MRI, presumably due to increased signal-to-noise and contrast-to-noise ratios, as shown in Figure 5. Despite the improvement in visualization of prostate morphology using T_2-weighted MRI at 3T, there is a need for increased specificity, as well as for obtaining "functional" cellular and metabolic information from prostate tissue. This can be achieved by including MRSI.[172] Adding MRSI can improve the reliable estimation of tumor margins and the extent of tumor infiltration into healthy tissue. However, a few benign and highly proliferative lesions can display relatively high tCho signals. In these cases, a differential diagnosis could be based on clinical information from other diagnostic scans.[40−42,173] Another clinical application for single-voxel ^{1}H MRS, as well as ^{1}H MRSI, is in treatment planning for radiation[174] or brachytherapy.[175]

3.2. Monitoring Therapy

Some of the most sought after goals in cancer management are the development of noninvasive biomarkers that predict risk, allow early identification, assist in the selection of treatment, and detect response.[176] Cancer cells have a remarkable ability to adapt and survive. Finding effective treatments against cancer depends upon identifying and attacking targets and pathways that are critically important for the cancer cell, with the additional caveat that each cancer represents an individual disease and that no two cancers may be alike. As more critical targets in cancer cells are revealed, this decade is witnessing a transition in cancer treatment from the "sledgehammer" approach of conventional chemo- and radiotherapy toward specific molecular targeting. The success of these molecular-targeted treatments critically depends upon the availability of noninvasive imaging techniques to select targeted therapies that would be most effective against a particular cancer and to detect response.[177] The identification of specific targets in cancer is also driving advances in novel image-guided platforms such as nanoparticles, liposomes, and microencapsulation devices to deliver small interfering RNA (siRNA)[178] or drugs to down-regulate these targets and pathways.

Detection of early therapeutic response following treatment with traditional cytotoxic drugs is critically important to minimize damage to normal tissue in nonresponding tumors and to alter the therapeutic strategy well before the full course of treatment. Single-voxel ^{1}H MRS and MRSI were found to be useful in assessing treatment response in brain,[31,32,179] breast,[5,164] and prostate[158] cancers. In breast cancer, several studies show that tCho has a high likelihood of detecting early response.[180] Response to primary systemic therapy (PST) of breast cancer was detected within 24 h of treatment by monitoring the change in tCho concentration,[5] as evident in Figure 6. In this study, MRI and MRS were performed on a 4T research MR scanner prior to treatment and within 24 h after treatment with combined doxorubicin and cyclophosphamide (see Figure 6). A lower tCho level compared to baseline was detected within 24 h with a further decrease after the fourth dose in patients who were objective responders (Figure 6). Total choline levels remained unchanged or increased in patients who were nonresponders (Figure 6).

Similar studies showed that the decrease in [tCho/citrate] ratios quantified from ^{1}H MR spectra could detect the response of prostate cancer to hormone-deprivation therapy[158,159] and cryosurgery[181] early on. Characteristic changes in choline phospholipid metabolites that were induced by anticancer treatments leading to apoptosis or necrosis were also reported.[15,182,183] Similarly, reduction of tCho has been associated with early response in lymphomas.[184] In some cancers, such as cervical cancer,[185] the tCho signal did not change following neoadjuvant treatment, but there was a reduction of tumor volume and the triglyceride signal.[185] The tumors were resected after treatment, but there were no

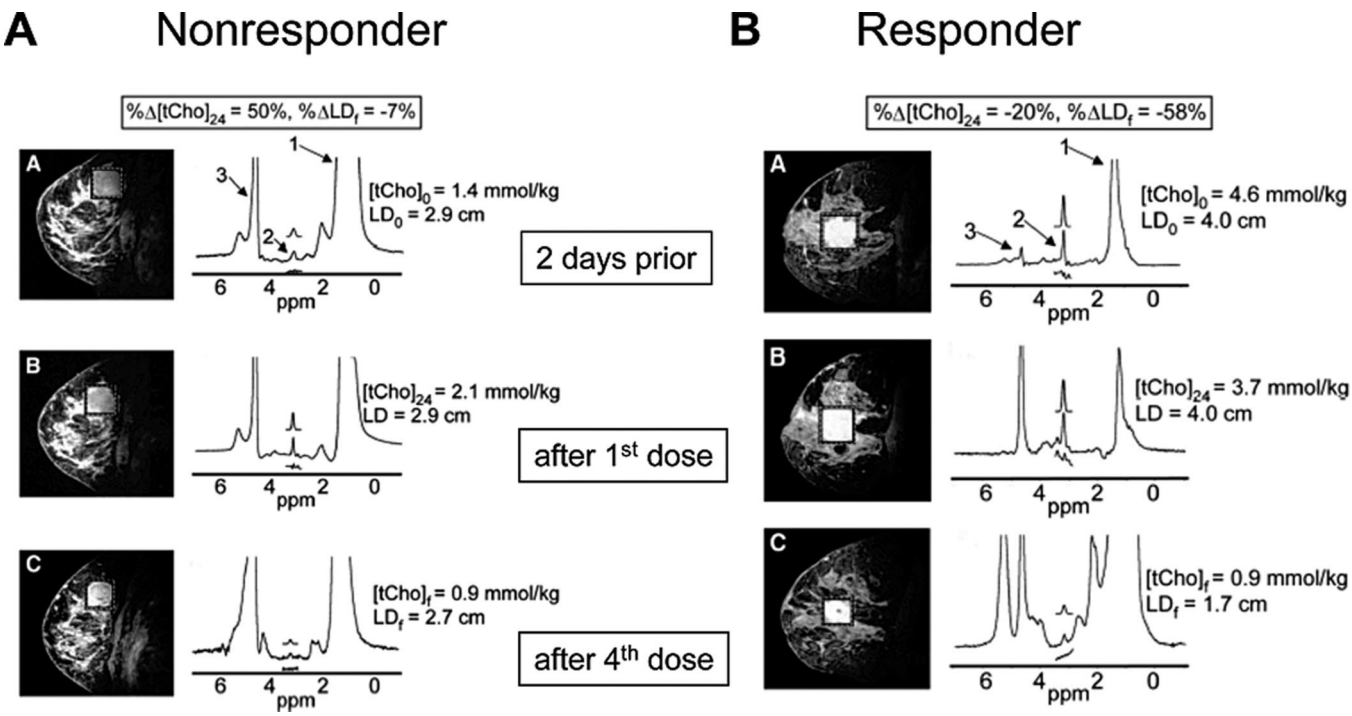

Figure 6. (A) Sagittal three-dimensional gadolinium-enhanced fat-suppressed MR images (left) and corresponding spectra (right) of the right breast in a 42-year-old *nonresponder* with invasive ductal carcinoma. (B) Sagittal three-dimensional gadolinium-enhanced fat-suppressed MR images (left) and corresponding spectra (right) of the right breast in a 43-year-old objective *responder* with invasive ductal carcinoma and positive lymph nodes. On MR images, boxes surrounding enhancing lesions depict spectroscopy voxels. The labeled spectral peaks rise from lipid (1), tCho (2), and water (3). Assignments: tCho, total choline-containing compounds; LD, longest diameter. Adapted from ref 5.

differences in survival in patients with or without neoadjuvant therapy and no survival advantage associated with reduction of tumor volume or decrease of triglycerides.[185]

As molecular targeted preclinical studies are revealing, while a decrease of tCho and PC is observed following treatment with molecular targeting of several pathways, e.g., mitogen activated protein kinase (MAPK),[186] fatty acid synthase,[187] and Bcr-Abl tyrosine kinase,[188] the decrease of tCho or PC cannot always be associated with response and depends upon the target selected. This was exemplified in a study showing that PC levels increased following histone deacetylase (HDAC) inhibition in cells.[189] However, PC levels did not change in tumors in vivo following HDAC inhibition.[189] This study also describes a novel fluorinated lysine derivative, which is a cleavable HDAC substrate that can be monitored by ^{19}F MRS to detect HDAC activity.[189]

Since one of the major causes of high PC in tumors is the increase in expression and activity of choline kinase (Chk), Chk presents an attractive target that can be exploited for cancer treatment.[9,190−193] An additional advantage of targeting Chk is that the decrease of PC and tCho resulting from its down-regulation can be detected noninvasively with ^{31}P or ^{1}H MRS.[190,191] Chk has been targeted with novel pharmacological inhibitors.[192,193] Pharmacological inhibition of Chk was found to result in growth arrest and apoptosis.[51,190] Chk has also been downregulated by RNA interference (RNAi).[9,191] RNAi is a naturally occurring process that mediates sequence-specific inhibition of gene expression.[194,195] Small interfering RNA (siRNA) is small double-stranded RNA of 19−23 nucleotides that can target virtually any gene and silence its expression.[194,195] Down-regulation of Chk-α with siRNA resulted in a significant reduction of cell proliferation and increased differentiation in highly invasive MDA-MB-231 human breast cancer cells, but not in nonmalignant immortalized MCF-12A mammary epithelial cells.[9] We subsequently used a lentiviral vector, injected intravenously, to deliver Chk-specific short-hairpin RNA (shRNA) in a breast cancer model.[191] In this study, down-regulation of Chk was monitored noninvasively by single-voxel ^{31}P MRS, as shown in Figure 7. We observed a reduction of PC and PME, which indicated that Chk was successfully down-regulated in this lentiviral Chk-targeted gene therapy.[191] Chk down-regulation also resulted in a reduction of cell proliferation and tumor growth (see Figure 7). These studies demonstrate the feasibility of future gene therapy trials targeting Chk in tumors.

Recently, ^{13}C MRSI of hyperpolarized ^{13}C-labeled substrates, such as [1-^{13}C]-pyruvate and [1,4-$^{13}C_2$]-fumarate, was used to detect treatment response in a murine lymphoma model.[70,196] The chemical structures of these compounds are shown in Table 2. Tumor response was detected by a decrease in the flux of hyperpolarized ^{13}C label between pyruvate and lactate in the case of [1-^{13}C]-pyruvate, and an increase of [1,4-$^{13}C_2$]-malate production in the case of [1,4-$^{13}C_2$]-fumarate. The increase of [1,4-$^{13}C_2$]-malate production was attributed to increased necrosis. These studies are important forerunners of the use of hyperpolarized ^{13}C-labeled substrates for detecting therapeutic response in tumors.

Poor drug delivery is another major problem in cancer chemotherapy, where MR methods can be used to directly determine the pharmacokinetics of a drug in the tumor or to provide surrogate indices of drug uptake.[197,198] Until recently, MR pharmacokinetic measurements of tumors in vivo were mainly restricted to fluorinated drugs such as [5-^{19}F]-fluorouracil (5-FU, for chemical structure see Table 3) detected by ^{19}F MRS,[199] because ^{19}F MRS has the advantage of relatively high sensitivity and no background signal. Fluorine-19 MRS was used to detect the uptake and metabolism of the chemotherapeutic agent 5-FU in liver metastases from colorectal cancer.[200] In preclinical studies,

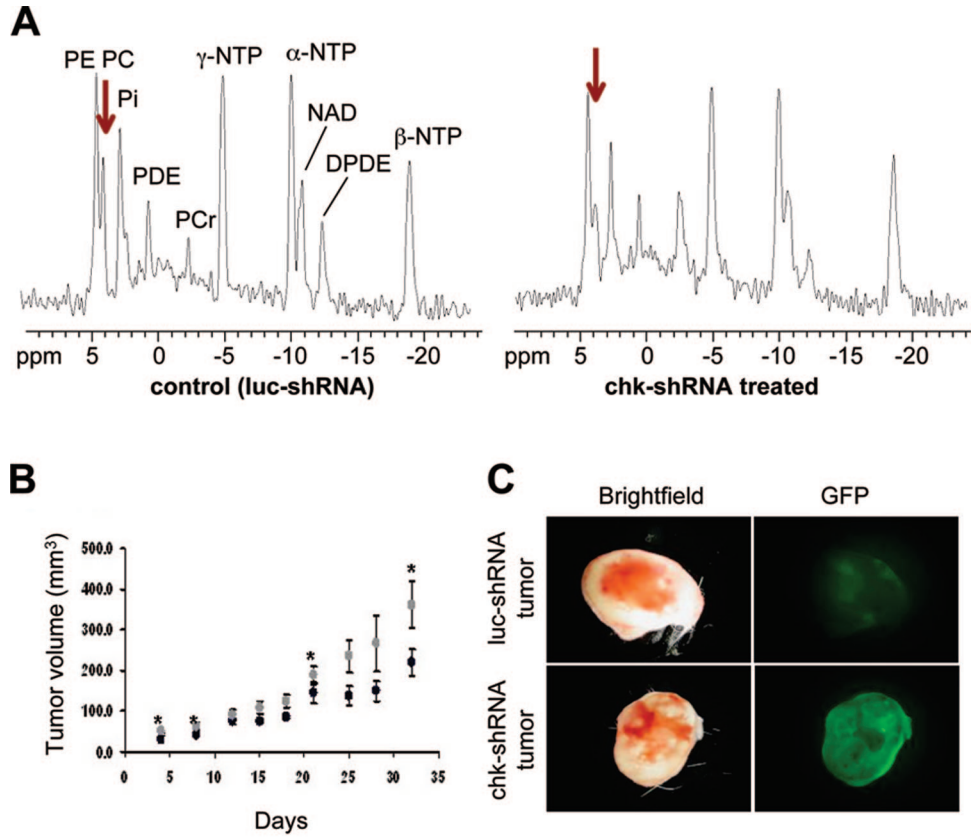

Figure 7. (A) Representative in vivo single-voxel ^{31}P MRS of MDA-MB-231 tumor xenografts following systemic delivery of lentivirus-expressing control shRNA that targets luciferase (luc-shRNA, left) or Chk-targeting shRNA (chk-shRNA, right). Chk-shRNA injection resulted in a significant reduction of PC (arrow) as compared to luc-shRNA. (B) Tumor growth rates were significantly reduced with lentivirus-mediated Chk targeting as compared to control luc-shRNA transduced controls. Tumor volume of luc-shRNA (gray circles, $n = 5$) and chk-shRNA (black circles, $n = 5$) transduced tumors is given in mm^3. Values represent mean and standard error. Asterisk indicates $p < 0.07$. (C) Representative brightfield and fluorescence photomicrographs of tumor sections showing distribution of enhanced green fluorescent protein (EGFP), which was expressed from the lentiviral vectors as delivery control, in luc-shRNA (upper panel) and chk-shRNA (lower panel) transduced tumors. This demonstrated successful delivery of lentiviruses into tumors following tail vein injection. Assignments: chk-shRNA, treated with lentivirus targeting choline kinase (chk) with specific short-hairpin RNA; DPDE, diphosphodiester; luc-shRNA; treated with lentivirus targeting luciferase (luc) with specific short-hairpin RNA as vector control; NAD, Nucleoside adenosine diphosphate; NTP, Nucleoside triphosphate; PC, phosphocholine; PDE, phosphodiester; PCr, phosphocreatine; PE, phosphoethanolamine; PME, phosphomonoester. Adapted from ref 191.

we recently reported on image-guided delivery of a prodrug enzyme, bacterial cytosine deaminase (bCD), that converts nontoxic [5-^{19}F]-fluorocytosine (5-FC, for chemical structure see Table 3) to 5-FU.[201] Visualization of the prodrug enzyme delivery was possible by conjugating it to poly-L-lysine functionalized with biotin, rhodamine, and Gd^{3+}-1,4,7,10-tetraazacyclododecane-1,4,7,10-tetraacetic acid (DOTA) for optical and MR imaging.[201] Image-guided timing of 5-FC prodrug administration to coincide with the maximum concentration of the enzyme in the tumor and the minimum concentration in normal tissue minimized damage from the active drug 5-FU in normal tissue while maximizing damage to cancer cells.[201] The conversion of the prodrug 5-FC to the active drug 5-FU was detected by ^{19}F MRS as shown in Figure 2.

For drugs lacking ^{19}F atoms, chemical ^{19}F-labeling may alter the physicochemical and pharmacological properties of the drug.[202,203] The feasibility of ^{13}C and ^{1}H MRS methods to detect drug uptake and distribution are, therefore, being explored.[204] Such approaches depend upon the labeled drug having at least one well-resolved, isolated peak and being delivered at doses high enough to be within the detection sensitivity of MRS.[205] Kato et al.[204] were able to image the intratumoral distribution of the ^{13}C-labeled anticancer agent Temozolomide (see Table 3 for chemical structure) by ^{1}H/^{13}C MRS. This ^{13}C MRSI study demonstrated that Temozolomide was heterogenously delivered to the tumor.[204] Temozolomide is used in the clinic for chemotherapy treatment of glioblastomas and anaplastic astrocytomas,[206] and the preclinical studies with brain cancer models demonstrate the potential use of ^{13}C MRS in detecting Temozolomide delivery in human cancers.[198]

4. Conclusions

Since the initial in vivo studies in the 1980s, multinuclear MRS has evolved into a highly versatile, noninvasive technique that is finding multiple applications in medical diagnosis, monitoring therapy, and research. Traditionally, MRS has provided biochemical characterization of pathological states. The increasing interface of chemistry with the fields of MRSI and molecular biology, and the resulting advances in theranostic contrast agent design, are providing new advances in the applications of MRS for molecular characterization and molecular-targeted medicine, especially in cancer. While sensitivity and spectral resolution continue to be limiting factors with this technique, the use of higher

field strengths and the application of techniques such as hyperpolarization are providing advances that minimize these limitations.

The heterogeneity of tumors and the resulting heterogeneity of tumor response to treatment frequently result in cancer being an intractable disease and make it imperative that each cancer is viewed individually in terms of the treatment selected and monitoring its response to treatment. The bench-to-bedside span of MRS, its ease of incorporation with MRI, and the multiparametric information that can be obtained make MRS a cornerstone technique for personalized medicine in cancer, in terms of predicting as well as detecting response to treatment.

5. Acknowledgments

Support from NIH P50 CA103175, P50 CA88843, P30 CA006973, U01 CA070095, U01 CA140204, R01 CA73850, R01 CA136576, R01 CA138515, R01 CA82337, R01 CA100184, R01 CA134695, R21 CA133288, and MD Stem Cells TEDCO 104026 is gratefully acknowledged.

6. References

(1) Brown, T. R.; Kincaid, B. M.; Ugurbil, K. *Proc. Natl. Acad. Sci. U.S.A.* **1982**, *79*, 3523.
(2) Haselgrove, J. C.; Subramanian, V. H.; Leigh, J. S., Jr.; Gyulai, L.; Chance, B. *Science* **1983**, *220*, 1170.
(3) Maudsley, A. A.; Hilal, S. K.; Perman, W. H.; Simon, H. E. *J. Magn. Reson.* **1983**, *51*, 147.
(4) Kurhanewicz, J.; Vigneron, D. B.; Males, R. G.; Swanson, M. G.; Yu, K. K.; Hricak, H. *Radiol. Clin. North Am.* **2000**, *38*, 115.
(5) Meisamy, S.; Bolan, P. J.; Baker, E. H.; Bliss, R. L.; Gulbahce, E.; Everson, L. I.; Nelson, M. T.; Emory, T. H.; Tuttle, T. M.; Yee, D.; Garwood, M. *Radiology* **2004**, *233*, 424.
(6) Baek, H. M.; Chen, J. H.; Nie, K.; Yu, H. J.; Bahri, S.; Mehta, R. S.; Nalcioglu, O.; Su, M. Y. *Radiology* **2009**, *251*, 653.
(7) Kumar, V.; Jagannathan, N. R.; Kumar, R.; Das, S. C.; Jindal, L.; Thulkar, S.; Gupta, S. D.; Dwivedi, S. N.; Roell, S.; Hemal, A. K.; Gupta, N. P. *Magn. Reson. Imaging* **2006**, *24*, 541.
(8) Glunde, K.; Jie, C.; Bhujwalla, Z. M. *Cancer Res.* **2004**, *64*, 4270.
(9) Glunde, K.; Raman, V.; Mori, N.; Bhujwalla, Z. M. *Cancer Res.* **2005**, *65*, 11034.
(10) Zhao, D.; Ran, S.; Constantinescu, A.; Hahn, E. W.; Mason, R. P. *Neoplasia* **2003**, *5*, 308.
(11) Kodibagkar, V. D.; Cui, W.; Merritt, M. E.; Mason, R. P. *Magn. Reson. Med.* **2006**, *55*, 743.
(12) Raman, V.; Artemov, D.; Pathak, A. P.; Winnard, P. T., Jr.; McNutt, S.; Yudina, A.; Bogdanov, A., Jr.; Bhujwalla, Z. M. *Cancer Res.* **2006**, *66*, 9929.
(13) Glunde, K.; Shah, T.; Winnard, P. T. J.; Raman, V.; Takagi, T.; Vesuna, F.; Artemov, D.; Bhujwalla, Z. M. *Cancer Res.* **2008**, *68*, 172.
(14) Penet, M. F.; Pathak, A. P.; Raman, V.; Ballesteros, P.; Artemov, D.; Bhujwalla, Z. M. *Cancer Res.* **2009**, *69*, 8822.
(15) Griffin, J. L.; Shockcor, J. P. *Nat. Rev. Cancer* **2004**, *4*, 551.
(16) Griffin, J. L.; Kauppinen, R. A. *J. Proteome Res.* **2007**, *6*, 498.
(17) Glunde, K.; Serkova, N. J. *Pharmacogenomics* **2006**, *7*, 1109.
(18) Costello, L. C.; Franklin, R. B. *Mol. Cell. Biochem.* **2005**, *280*, 1.
(19) Griffin, J. L.; Kauppinen, R. A. *FEBS J.* **2007**, *274*, 1132.
(20) Millis, K.; Weybright, P.; Campbell, N.; Fletcher, J. A.; Fletcher, C. D.; Cory, D. G.; Singer, S. *Magn. Reson. Med.* **1999**, *41*, 257.
(21) Swanson, M. G.; Vigneron, D. B.; Tabatabai, Z. L.; Males, R. G.; Schmitt, L.; Carroll, P. R.; James, J. K.; Hurd, R. E.; Kurhanewicz, J. *Magn. Reson. Med.* **2003**, *50*, 944.
(22) Swanson, M. G.; Zektzer, A. S.; Tabatabai, Z. L.; Simko, J.; Jarso, S.; Keshari, K. R.; Schmitt, L.; Carroll, P. R.; Shinohara, K.; Vigneron, D. B.; Kurhanewicz, J. *Magn. Reson. Med.* **2006**, *55*, 1257.
(23) Barker, P. B.; Glickson, J. D.; Bryan, R. N. *Top. Magn. Reson. Imaging* **1993**, *5*, 32.
(24) Pouwels, P. J.; Frahm, J. *Magn. Reson. Med.* **1998**, *39*, 53.
(25) Ross, B.; Michaelis, T. *Magn. Reson. Q* **1994**, *10*, 191.
(26) Chang, L.; McBride, D.; Miller, B. L.; Cornford, M.; Booth, R. A.; Buchthal, S. D.; Ernst, T. M.; Jenden, D. *J. Neuroimaging* **1995**, *5*, 157.
(27) Tzika, A. A.; Cheng, L. L.; Goumnerova, L.; Madsen, J. R.; Zurakowski, D.; Astrakas, L. G.; Zarifi, M. K.; Scott, R. M.; Anthony, D. C.; Gonzalez, R. G.; Black, P. M. *J. Neurosurg.* **2002**, *96*, 1023.
(28) Nelson, S. J. *Magn. Reson. Med.* **2001**, *46*, 228.
(29) Howe, F. A.; Barton, S. J.; Cudlip, S. A.; Stubbs, M.; Saunders, D. E.; Murphy, M.; Wilkins, P.; Opstad, K. S.; Doyle, V. L.; McLean, M. A.; Bell, B. A.; Griffiths, J. R. *Magn. Reson. Med.* **2003**, *49*, 223.
(30) Murphy, M.; Loosemore, A.; Clifton, A. G.; Howe, F. A.; Tate, A. R.; Cudlip, S. A.; Wilkins, P. R.; Griffiths, J. R.; Bell, B. A. *Br. J. Neurosurg.* **2002**, *16*, 329.
(31) Lindskog, M.; Spenger, C.; Klason, T.; Jarvet, J.; Graslund, A.; Johnsen, J. I.; Ponthan, F.; Douglas, L.; Nordell, B.; Kogner, P. *Cancer Lett.* **2005**, *228*, 247.
(32) Jenkinson, M. D.; Smith, T. S.; Joyce, K.; Fildes, D.; du Plessis, D. G.; Warnke, P. C.; Walker, C. *Neurology* **2005**, *64*, 2085.
(33) Jeun, S. S.; Kim, M. C.; Kim, B. S.; Lee, J. M.; Chung, S. T.; Oh, C. H.; Lee, S. Y.; Choe, B. Y. *Clin. Imaging* **2005**, *29*, 10.
(34) McKnight, T. R. *Semin. Oncol.* **2004**, *31*, 605.
(35) Narayan, P.; Kurhanewicz, J. *Prostate Suppl.* **1992**, *4*, 43.
(36) Schick, F.; Bongers, H.; Kurz, S.; Jung, W. I.; Pfeffer, M.; Lutz, O. *Magn. Reson. Med.* **1993**, *29*, 38.
(37) Kurhanewicz, J.; Vigneron, D. B.; Hricak, H.; Narayan, P.; Carroll, P.; Nelson, S. J. *Radiology* **1996**, *198*, 795.
(38) Menard, C.; Smith, I. C.; Somorjai, R. L.; Leboldus, L.; Patel, R.; Littman, C.; Robertson, S. J.; Bezabeh, T. *Int. J. Radiat. Oncol. Biol. Phys.* **2001**, *50*, 317.
(39) Jagannathan, N. R.; Singh, M.; Govindaraju, V.; Raghunathan, P.; Coshic, O.; Julka, P. K.; Rath, G. K. *NMR Biomed.* **1998**, *11*, 414.
(40) Roebuck, J. R.; Cecil, K. M.; Schnall, M. D.; Lenkinski, R. E. *Radiology* **1998**, *209*, 269.
(41) Yeung, D. K.; Cheung, H. S.; Tse, G. M. *Radiology* **2001**, *220*, 40.
(42) Jacobs, M. A.; Barker, P. B.; Bottomley, P. A.; Bhujwalla, Z.; Bluemke, D. A. *J. Magn. Reson. Imaging* **2004**, *19*, 68.
(43) Bolan, P. J.; Meisamy, S.; Baker, E. H.; Lin, J.; Emory, T.; Nelson, M.; Everson, L. I.; Yee, D.; Garwood, M. *Magn. Reson. Med.* **2003**, *50*, 1134.
(44) Meisamy, S.; Bolan, P. J.; Baker, E. H.; Pollema, M. G.; Le, C. T.; Kelcz, F.; Lechner, M. C.; Luikens, B. A.; Carlson, R. A.; Brandt, K. R.; Amrami, K. K.; Nelson, M. T.; Everson, L. I.; Emory, T. H.; Tuttle, T. M.; Yee, D.; Garwood, M. *Radiology* **2005**, *236*, 465.
(45) Stanwell, P.; Gluch, L.; Clark, D.; Tomanek, B.; Baker, L.; Giuffre, B.; Lean, C.; Malycha, P.; Mountford, C. *Eur. Radiol.* **2005**, *15*, 1037.
(46) Baik, H. M.; Su, M. Y.; Yu, H.; Nalcioglu, O.; Mehta, R. *Magma* **2006**, *19*, 96.
(47) Ramirez de Molina, A.; Gallego-Ortega, D.; Sarmentero, J.; Banez-Coronel, M.; Martin-Cantalejo, Y.; Lacal, J. C. *Cancer Res.* **2005**, *65*, 5647.
(48) Ramirez de Molina, A.; Gutierrez, R.; Ramos, M. A.; Silva, J. M.; Silva, J.; Bonilla, F.; Sanchez, J. J.; Lacal, J. C. *Oncogene* **2002**, *21*, 4317.
(49) Ramirez de Molina, A.; Penalva, V.; Lucas, L.; Lacal, J. C. *Oncogene* **2002**, *21*, 937.
(50) Ramirez de Molina, A.; Rodriguez-Gonzalez, A.; Gutierrez, R.; Martinez-Pineiro, L.; Sanchez, J.; Bonilla, F.; Rosell, R.; Lacal, J. *Biochem. Biophys. Res. Commun.* **2002**, *296*, 580.
(51) Rodriguez-Gonzalez, A.; Ramirez de Molina, A.; Fernandez, F.; Lacal, J. C. *Oncogene* **2004**, *23*, 8247.
(52) Artemov, D.; Bhujwalla, Z. M.; Glickson, J. D. *Magn. Reson. Med.* **1995**, *33*, 151.
(53) van Zijl, P. C.; Chesnick, A. S.; DesPres, D.; Moonen, C. T.; Ruiz-Cabello, J.; van Gelderen, P. *Magn. Reson. Med.* **1993**, *30*, 544.
(54) Vander Heiden, M. G.; Cantley, L. C.; Thompson, C. B. *Science* **2009**, *324*, 1029.
(55) Kim, J. W.; Dang, C. V. *Cancer Res.* **2006**, *66*, 8927.
(56) Semenza, G. L. *Biochem. J.* **2007**, *405*, 1.
(57) Vaupel, P.; Kallinowski, F.; Okunieff, P. *Cancer Res.* **1989**, *49*, 6449.
(58) Vaupel, P.; Okunieff, P.; Kallinowski, F.; Neuringer, L. J. *Radiat. Res.* **1989**, *120*, 477.
(59) Medina, R. A.; Owen, G. I. *Biol. Res.* **2002**, *35*, 9.
(60) Macheda, M. L.; Rogers, S.; Best, J. D. *J. Cell Physiol.* **2005**, *202*, 654.
(61) Rivenzon-Segal, D.; Margalit, R.; Degani, H. *Am. J. Physiol. Endocrinol. Metab.* **2002**, *283*, E623.
(62) Terpstra, M.; High, W. B.; Luo, Y.; de Graaf, R. A.; Merkle, H.; Garwood, M. *NMR Biomed.* **1996**, *9*, 185.
(63) Nielsen, F. U.; Daugaard, P.; Bentzen, L.; Stodkilde-Jorgensen, H.; Overgaard, J.; Horsman, M. R.; Maxwell, R. J. *Cancer Res.* **2001**, *61*, 5318.
(64) Constantinidis, I.; Chatham, J. C.; Wehrle, J. P.; Glickson, J. D. *Magn. Reson. Med.* **1991**, *20*, 17.
(65) Bhujwalla, Z. M.; Constantinidis, I.; Chatham, J. C.; Wehrle, J. P.; Glickson, J. D. *Int. J. Radiat. Oncol. Biol. Phys.* **1992**, *22*, 95.

(66) Schupp, D. G.; Merkle, H.; Ellermann, J. M.; Ke, Y.; Garwood, M. *Magn. Reson. Med.* **1993**, *30*, 18.
(67) Artemov, D.; Bhujwalla, Z. M.; Pilatus, U.; Glickson, J. D. *NMR Biomed.* **1998**, *11*, 395.
(68) Bouzier, A. K.; Quesson, B.; Valeins, H.; Canioni, P.; Merle, M. *J. Neurochem.* **1999**, *72*, 2445.
(69) Ardenkjaer-Larsen, J. H.; Fridlund, B.; Gram, A.; Hansson, G.; Hansson, L.; Lerche, M. H.; Servin, R.; Thaning, M.; Golman, K. *Proc. Natl. Acad. Sci. U.S.A.* **2003**, *100*, 10158.
(70) Day, S. E.; Kettunen, M. I.; Gallagher, F. A.; Hu, D. E.; Lerche, M.; Wolber, J.; Golman, K.; Ardenkjaer-Larsen, J. H.; Brindle, K. M. *Nat. Med.* **2007**, *13*, 1382.
(71) Albers, M. J.; Bok, R.; Chen, A. P.; Cunningham, C. H.; Zierhut, M. L.; Zhang, V. Y.; Kohler, S. J.; Tropp, J.; Hurd, R. E.; Yen, Y. F.; Nelson, S. J.; Vigneron, D. B.; Kurhanewicz, J. *Cancer Res.* **2008**, *68*, 8607.
(72) Abragam, A. A.; Proctor, W. G. *Phys. Rev.* **1958**, *109*.
(73) Goldman, M.; Johannesson, H.; Axelsson, O.; Karlsson, M. *Magn. Reson. Imaging* **2005**, *23*, 153.
(74) Johansson, E.; Olsson, L. E.; Mansson, S.; Petersson, J. S.; Golman, K.; Stahlberg, F.; Wirestam, R. *Magn. Reson. Med.* **2004**, *52*, 1043.
(75) Negendank, W. *NMR Biomed.* **1992**, *5*, 303.
(76) Podo, F. *NMR Biomed.* **1999**, *12*, 413.
(77) Ronen, S. M.; Leach, M. O. *Breast Cancer Res.* **2001**, *3*, 36.
(78) Ackerstaff, E.; Glunde, K.; Bhujwalla, Z. M. *J. Cell. Biochem.* **2003**, *90*, 525.
(79) Franks, S. E.; Smith, M. R.; Arias-Mendoza, F.; Shaller, C.; Padavic-Shaller, K.; Kappler, F.; Zhang, Y.; Negendank, W. G.; Brown, T. R. *Leuk. Res.* **2002**, *26*, 919.
(80) Aboagye, E. O.; Bhujwalla, Z. M. *Cancer Res.* **1999**, *59*, 80.
(81) Iorio, E.; Mezzanzanica, D.; Alberti, P.; Spadaro, F.; Ramoni, C.; D'Ascenzo, S.; Millimaggi, D.; Pavan, A.; Dolo, V.; Canevari, S.; Podo, F. *Cancer Res.* **2005**, *65*, 9369.
(82) Arias-Mendoza, F.; Payne, G. S.; Zakian, K. L.; Schwarz, A. J.; Stubbs, M.; Stoyanova, R.; Ballon, D.; Howe, F. A.; Koutcher, J. A.; Leach, M. O.; Griffiths, J. R.; Heerschap, A.; Glickson, J. D.; Nelson, S. J.; Evelhoch, J. L.; Charles, H. C.; Brown, T. R. *NMR Biomed.* **2006**, *19*, 504.
(83) Albers, M. J.; Krieger, M. D.; Gonzalez-Gomez, I.; Gilles, F. H.; McComb, J. G.; Nelson, M. D., Jr.; Bluml, S. *Magn. Reson. Med.* **2005**, *53*, 22.
(84) Klomp, D. W.; Wijnen, J. P.; Scheenen, T. W.; Heerschap, A. *Magn. Reson. Med.* **2008**, *60*, 1298.
(85) Katz-Brull, R.; Degani, H. *Anticancer Res.* **1996**, *16*, 1375.
(86) Eliyahu, G.; Kreizman, T.; Degani, H. *Int. J. Cancer* **2007**, *120*, 1721.
(87) Noh, D. Y.; Ahn, S. J.; Lee, R. A.; Park, I. A.; Kim, J. H.; Suh, P. G.; Ryu, S. H.; Lee, K. H.; Han, J. S. *Cancer Lett.* **2000**, *161*, 207.
(88) Foster, D. A.; Xu, L. *Mol. Cancer Res.* **2003**, *1*, 789.
(89) Gillies, R. J.; Morse, D. L. *Annu. Rev. Biomed. Eng.* **2005**, *7*, 287.
(90) Hakumaki, J. M.; Poptani, H.; Sandmair, A. M.; Yla-Herttuala, S.; Kauppinen, R. A. *Nat. Med.* **1999**, *5*, 1323.
(91) Engelmann, J.; Henke, J.; Willker, W.; Kutscher, B.; Nossner, G.; Engel, J.; Leibfritz, D. *Anticancer Res.* **1996**, *16*, 1429.
(92) Al-Saffar, N. M.; Titley, J. C.; Robertson, D.; Clarke, P. A.; Jackson, L. E.; Leach, M. O.; Ronen, S. M. *Br. J. Cancer* **2002**, *86*, 963.
(93) Barba, I.; Cabanas, M. E.; Arus, C. *Cancer Res.* **1999**, *59*, 1861.
(94) Callies, R.; Sri-Pathmanathan, R. M.; Ferguson, D. Y.; Brindle, K. M. *Magn. Reson. Med.* **1993**, *29*, 546.
(95) Schmitz, J. E.; Kettunen, M. I.; Hu, D. E.; Brindle, K. M. *Magn. Reson. Med.* **2005**, *54*, 43.
(96) Ackerman, J. J.; Grove, T. H.; Wong, G. G.; Gadian, D. G.; Radda, G. K. *Nature* **1980**, *283*, 167.
(97) Griffiths, J. R.; Cady, E.; Edwards, R. H.; McCready, V. R.; Wilkie, D. R.; Wiltshaw, E. *Lancet* **1983**, *1*, 1435.
(98) Bottomley, P. A.; Charles, H. C.; Roemer, P. B.; Flamig, D.; Engeseth, H.; Edelstein, W. A.; Mueller, O. M. *Magn. Reson. Med.* **1988**, *7*, 319.
(99) Hardy, C. J.; Bottomley, P. A.; Roemer, P. B.; Redington, R. W. *Magn. Reson. Med.* **1988**, *8*, 104.
(100) Okunieff, P. G.; Koutcher, J. A.; Gerweck, L.; McFarland, E.; Hitzig, B.; Urano, M.; Brady, T.; Neuringer, L.; Suit, H. D. *Int. J. Radiat. Oncol. Biol. Phys.* **1986**, *12*, 793.
(101) Li, S. J.; Wehrle, J. P.; Rajan, S. S.; Steen, R. G.; Glickson, J. D.; Hilton, J. *Cancer Res.* **1988**, *48*, 4736.
(102) Kallman, R. F. *Radiology* **1972**, *105*, 135.
(103) Tozer, G. M.; Griffiths, J. R. *NMR Biomed.* **1992**, *5*, 279.
(104) Cheng, L. L.; Chang, I. W.; Louis, D. N.; Gonzalez, R. G. *Cancer Res.* **1998**, *58*, 1825.
(105) Cheng, L. L.; Chang, I. W.; Smith, B. L.; Gonzalez, R. G. *J. Magn. Reson.* **1998**, *135*, 194.
(106) Cheng, L. L.; Burns, M. A.; Taylor, J. L.; He, W.; Halpern, E. F.; McDougal, W. S.; Wu, C. L. *Cancer Res.* **2005**, *65*, 3030.
(107) Sitter, B.; Lundgren, S.; Bathen, T. F.; Halgunset, J.; Fjosne, H. E.; Gribbestad, I. S. *NMR Biomed.* **2006**, *19*, 30.
(108) Sitter, B.; Sonnewald, U.; Spraul, M.; Fjosne, H. E.; Gribbestad, I. S. *NMR Biomed.* **2002**, *15*, 327.
(109) Martinez-Bisbal, M. C.; Marti-Bonmati, L.; Piquer, J.; Revert, A.; Ferrer, P.; Llacer, J. L.; Piotto, M.; Assemat, O.; Celda, B. *NMR Biomed.* **2004**, *17*, 191.
(110) Payne, G. S.; Troy, H.; Vaidya, S. J.; Griffiths, J. R.; Leach, M. O.; Chung, Y. L. NMR Biomed. 2006.
(111) Alger, J. R.; Shulman, R. G. *Q. Rev. Biophys.* **1984**, *17*, 83.
(112) Ward, K. M.; Aletras, A. H.; Balaban, R. S. *J. Magn. Reson.* **2000**, *143*, 79.
(113) Zhou, J.; Payen, J. F.; Wilson, D. A.; Traystman, R. J.; van Zijl, P. C. *Nat. Med.* **2003**, *9*, 1085.
(114) Gilad, A. A.; McMahon, M. T.; Walczak, P.; Winnard, P. T., Jr.; Raman, V.; van Laarhoven, H. W.; Skoglund, C. M.; Bulte, J. W.; van Zijl, P. C. *Nat. Biotechnol.* **2007**, *25*, 217.
(115) McMahon, M. T.; Gilad, A. A.; DeLiso, M. A.; Berman, S. M.; Bulte, J. W.; van Zijl, P. C. *Magn. Reson. Med.* **2008**, *60*, 803.
(116) Jain, R. K. *Cancer Res.* **1988**, *48*, 2641.
(117) Gatenby, R. A.; Gillies, R. J. *Nat. Rev. Cancer* **2004**, *4*, 891.
(118) Lunt, S. J.; Chaudary, N.; Hill, R. P. *Clin. Exp. Metastasis* **2009**, *26*, 19.
(119) Rockwell, S.; Dobrucki, I. T.; Kim, E. Y.; Marrison, S. T.; Vu, V. T. *Curr. Mol. Med.* **2009**, *9*, 442.
(120) Parhami, P.; Fung, B. M. *J. Phys. Chem.* **1983**, *87*, 1928.
(121) Zhao, D.; Jiang, L.; Mason, R. P. *Methods Enzymol.* **2004**, *386*, 378.
(122) Dardzinski, B. J.; Sotak, C. H. *Magn. Reson. Med.* **1994**, *32*, 88.
(123) Jordan, B. F.; Cron, G. O.; Gallez, B. *Magn. Reson. Med.* **2009**, *61*, 634.
(124) Baldwin, N. J.; Ng, T. C. *Magn. Reson. Imaging* **1996**, *14*, 541.
(125) Mason, R. P.; Antich, P. P.; Babcock, E. E.; Constantinescu, A.; Peschke, P.; Hahn, E. W. *Int. J. Radiat. Oncol. Biol. Phys.* **1994**, *29*, 95.
(126) Kodibagkar, V. D.; Wang, X.; Mason, R. P. *Front. Biosci.* **2008**, *13*, 1371.
(127) Kodibagkar, V. D.; Wang, X.; Pacheco-Torres, J.; Gulaka, P.; Mason, R. P. *NMR Biomed.* **2008**, *21*, 899.
(128) Aboagye, E. O.; Kelson, A. B.; Tracy, M.; Workman, P. *Anti-Cancer Drug Des.* **1998**, *13*, 703.
(129) Procissi, D.; Claus, F.; Burgman, P.; Koziorowski, J.; Chapman, J. D.; Thakur, S. B.; Matei, C.; Ling, C. C.; Koutcher, J. A. *Clin. Cancer Res.* **2007**, *13*, 3738.
(130) Varghese, A. J.; Gulyas, S.; Mohindra, J. K. *Cancer Res.* **1976**, *36*, 3761.
(131) Kizaka-Kondoh, S.; Konse-Nagasawa, H. *Cancer Sci* **2009**, *100*, 1366.
(132) Laughlin, K. M.; Evans, S. M.; Jenkins, W. T.; Tracy, M.; Chan, C. Y.; Lord, E. M.; Koch, C. J. *J. Pharmacol. Exp. Ther.* **1996**, *277*, 1049.
(133) Moon, R. B.; Richards, J. H. *J. Biol. Chem.* **1973**, *248*, 7276.
(134) Stubbs, M.; Bhujwalla, Z. M.; Tozer, G. M.; Rodrigues, L. M.; Maxwell, R. J.; Morgan, R.; Howe, F. A.; Griffiths, J. R. *NMR Biomed.* **1992**, *5*, 351.
(135) Griffiths, J. R. *Br. J. Cancer* **1991**, *64*, 425.
(136) Gillies, R. J.; Liu, Z.; Bhujwalla, Z. M. *Am. J. Physiol.* **1994**, *267*, C195.
(137) van Sluis, R.; Bhujwalla, Z. M.; Raghunand, N.; Ballesteros, P.; Alvarez, J.; Cerdan, S.; Galons, J. P.; Gillies, R. J. *Magn. Reson. Med.* **1999**, *41*, 743.
(138) Martinez-Zaguilan, R.; Seftor, E. A.; Seftor, R. E.; Chu, Y. W.; Gillies, R. J.; Hendrix, M. J. *Clin. Exp. Metastasis* **1996**, *14*, 176.
(139) Raghunand, N.; Mahoney, B.; van Sluis, R.; Baggett, B.; Gillies, R. J. *Neoplasia* **2001**, *3*, 227.
(140) Robey, I. F.; Baggett, B. K.; Kirkpatrick, N. D.; Roe, D. J.; Dosescu, J.; Sloane, B. F.; Hashim, A. I.; Morse, D. L.; Raghunand, N.; Gatenby, R. A.; Gillies, R. J. *Cancer Res.* **2009**, *69*, 2260.
(141) Gil, S.; Zaderenzo, P.; Cruz, F.; Cerdan, S.; Ballesteros, P. *Bioorg. Med. Chem.* **1994**, *2*, 305.
(142) Bhujwalla, Z. M.; Artemov, D.; Ballesteros, P.; Cerdan, S.; Gillies, R. J.; Solaiyappan, M. *NMR Biomed.* **2002**, *15*, 114.
(143) Ojugo, A. S.; McSheehy, P. M.; McIntyre, D. J.; McCoy, C.; Stubbs, M.; Leach, M. O.; Judson, I. R.; Griffiths, J. R. *NMR Biomed.* **1999**, *12*, 495.
(144) Mason, R. P. *Curr. Med. Chem.* **1999**, *6*, 481.
(145) Garcia-Martin, M. L.; Martinez, G. V.; Raghunand, N.; Sherry, A. D.; Zhang, S.; Gillies, R. J. *Magn. Reson. Med.* **2006**, *55*, 309.
(146) Provent, P.; Benito, M.; Hiba, B.; Farion, R.; Lopez-Larrubia, P.; Ballesteros, P.; Remy, C.; Segebarth, C.; Cerdan, S.; Coles, J. A.; Garcia-Martin, M. L. *Cancer Res.* **2007**, *67*, 7638.
(147) Gil, M. S.; Cruz, F.; Cerdan, S.; Ballesteros, P. *Bioorg. Med. Chem. Lett.* **1992**, *2*, 1717.
(148) Garcia-Martin, M. L.; Herigault, G.; Remy, C.; Farion, R.; Ballesteros, P.; Coles, J. A.; Cerdan, S.; Ziegler, A. *Cancer Res.* **2001**, *61*, 6524.

(149) Ward, K. M.; Balaban, R. S. *Magn. Reson. Med.* **2000**, *44*, 799.
(150) Aime, S.; Barge, A.; Delli Castelli, D.; Fedeli, F.; Mortillaro, A.; Nielsen, F. U.; Terreno, E. *Magn. Reson. Med.* **2002**, *47*, 639.
(151) Woods, M.; Woessner, D. E.; Sherry, A. D. *Chem. Soc. Rev.* **2006**, *35*, 500.
(152) Cai, S.; Seu, C.; Kovacs, Z.; Sherry, A. D.; Chen, Y. *J. Am. Chem. Soc.* **2006**, *128*, 13474.
(153) Yoo, B.; Pagel, M. D. *Front. Biosci.* **2008**, *13*, 1733.
(154) Gianolio, E.; Napolitano, R.; Fedeli, F.; Arena, F.; Aime, S. *Chem. Commun.* **2009**, 6044.
(155) Gallagher, F. A.; Kettunen, M. I.; Day, S. E.; Hu, D. E.; Ardenkjaer-Larsen, J. H.; Zandt, R.; Jensen, P. R.; Karlsson, M.; Golman, K.; Lerche, M. H.; Brindle, K. M. *Nature* **2008**, *453*, 940.
(156) Gill, S. S.; Thomas, D. G.; Van Bruggen, N.; Gadian, D. G.; Peden, C. J.; Bell, J. D.; Cox, I. J.; Menon, D. K.; Iles, R. A.; Bryant, D. J.; et al. *J. Comput. Assisted Tomogr.* **1990**, *14*, 497.
(157) Weiner, M. W.; Hetherington, H.; Hubesch, B.; Karczmar, G.; Massie, B.; Maudsley, A.; Meyerhoff, D. J.; Sappey-Marinier, D.; Schaefer, S.; Twieg, D. B.; et al. *NMR Biomed.* **1989**, *2*, 290.
(158) Kurhanewicz, J.; Vigneron, D. B.; Nelson, S. J. *Neoplasia* **2000**, *2*, 166.
(159) Mueller-Lisse, U. G.; Swanson, M. G.; Vigneron, D. B.; Hricak, H.; Bessette, A.; Males, R. G.; Wood, P. J.; Noworolski, S.; Nelson, S. J.; Barken, I.; Carroll, P. R.; Kurhanewicz, J. *Magn. Reson. Med.* **2001**, *46*, 49.
(160) Jacobs, M. A.; Barker, P. B.; Argani, P.; Ouwerkerk, R.; Bhujwalla, Z. M.; Bluemke, D. B. *J. Magn. Reson. Imaging* **2005**, *21*, 23.
(161) Lehnhardt, F. G.; Bock, C.; Rohn, G.; Ernestus, R. I.; Hoehn, M. *NMR Biomed.* **2005**, *18*, 371.
(162) Mountford, C. E.; Somorjai, R. L.; Malycha, P.; Gluch, L.; Lean, C.; Russell, P.; Barraclough, B.; Gillett, D.; Himmelreich, U.; Dolenko, B.; Nikulin, A. E.; Smith, I. C. *Br. J. Surg.* **2001**, *88*, 1234.
(163) Li, X.; Lu, Y.; Pirzkall, A.; McKnight, T.; Nelson, S. J. *J. Magn. Reson. Imaging* **2002**, *16*, 229.
(164) Manton, D. J.; Chaturvedi, A.; Hubbard, A.; Lind, M. J.; Lowry, M.; Maraveyas, A.; Pickles, M. D.; Tozer, D. J.; Turnbull, L. W. *Br. J. Cancer* **2006**, *94*, 427.
(165) Hu, J.; Vartanian, S. A.; Xuan, Y.; Latif, Z.; Soulen, R. L. *Magn. Reson. Imaging* **2005**, *23*, 571.
(166) Laprie, A.; Pirzkall, A.; Haas-Kogan, D. A.; Cha, S.; Banerjee, A.; Le, T. P.; Lu, Y.; Nelson, S.; McKnight, T. R. *Int. J. Radiat. Oncol. Biol. Phys.* **2005**, *62*, 20.
(167) Taylor, J. S.; Langston, J. W.; Reddick, W. E.; Kingsley, P. B.; Ogg, R. J.; Pui, M. H.; Kun, L. E.; Jenkins, J. J., 3rd; Chen, G.; Ochs, J. J.; Sanford, R. A.; Heideman, R. L. *Int. J. Radiat. Oncol. Biol. Phys.* **1996**, *36*, 1251.
(168) Wald, L. L.; Nelson, S. J.; Day, M. R.; Noworolski, S. E.; Henry, R. G.; Huhn, S. L.; Chang, S.; Prados, M. D.; Sneed, P. K.; Larson, D. A.; Wara, W. M.; McDermott, M.; Dillon, W. P.; Gutin, P. H.; Vigneron, D. B. *J. Neurosurg.* **1997**, *87*, 525.
(169) Kurhanewicz, J.; Swanson, M. G.; Nelson, S. J.; Vigneron, D. B. *J. Magn. Reson. Imaging* **2002**, *16*, 451.
(170) Carroll, P. R.; Coakley, F. V.; Kurhanewicz, J. *Rev. Urol.* **2006**, *8* (Suppl 1), S4.
(171) Hricak, H.; Williams, R. D.; Spring, D. B.; Moon, K. L., Jr.; Hedgcock, M. W.; Watson, R. A.; Crooks, L. E. *Am J Roentgenol.* **1983**, *141*, 1101.
(172) Jacobs, M. A.; Ouwerkerk, R.; Petrowski, K.; Macura, K. J. *Top. Magn. Reson. Imaging* **2008**, *19*, 261.
(173) Loening, N. M.; Chamberlin, A. M.; Zepeda, A. G.; Gonzalez, R. G.; Cheng, L. L. *NMR Biomed.* **2005**, *18*, 413.
(174) Nelson, S. J.; Graves, E.; Pirzkall, A.; Li, X.; Antiniw Chan, A.; Vigneron, D. B.; McKnight, T. R. *J. Magn. Reson. Imaging* **2002**, *16*, 464.
(175) Zaider, M.; Zelefsky, M. J.; Lee, E. K.; Zakian, K. L.; Amols, H. I.; Dyke, J.; Cohen, G.; Hu, Y.; Endi, A. K.; Chui, C.; Koutcher, J. A. *Int. J. Radiat. Oncol. Biol. Phys.* **2000**, *47*, 1085.
(176) Sawyers, C. L. *Nature* **2008**, *452*, 548.
(177) Weissleder, R.; Pittet, M. J. *Nature* **2008**, *452*, 580.
(178) Medarova, Z.; Pham, W.; Farrar, C.; Petkova, V.; Moore, A. *Nat. Med.* **2007**, *13*, 372.
(179) Law, M.; Cha, S.; Knopp, E. A.; Johnson, G.; Arnett, J.; Litt, A. W. *Radiology* **2002**, *222*, 715.
(180) Haddadin, I. S.; McIntosh, A.; Meisamy, S.; Corum, C.; Styczynski Snyder, A. L.; Powell, N. J.; Nelson, M. T.; Yee, D.; Garwood, M.; Bolan, P. J. *NMR Biomed.* **2009**, *22*, 65.
(181) Kurhanewicz, J.; Vigneron, D. B.; Hricak, H.; Parivar, F.; Nelson, S. J.; Shinohara, K.; Carroll, P. R. *Radiology* **1996**, *200*, 489.
(182) Gillies, R. J.; Bhujwalla, Z. M.; Evelhoch, J.; Garwood, M.; Neeman, M.; Robinson, S. P.; Sotak, C. H.; Van Der Sanden, B. *Neoplasia* **2000**, *2*, 139.
(183) Evelhoch, J. L.; Gillies, R. J.; Karczmar, G. S.; Koutcher, J. A.; Maxwell, R. J.; Nalcioglu, O.; Raghunand, N.; Ronen, S. M.; Ross, B. D.; Swartz, H. M. *Neoplasia* **2000**, *2*, 152.
(184) Schwarz, A. J.; Maisey, N. R.; Collins, D. J.; Cunningham, D.; Huddart, R.; Leach, M. O. *Br. J. Radiol.* **2002**, *75*, 959.
(185) deSouza, N. M.; Soutter, W. P.; Rustin, G.; Mahon, M. M.; Jones, B.; Dina, R.; McIndoe, G. A. *Br. J. Cancer* **2004**, *90*, 2326.
(186) Beloueche-Babari, M.; Jackson, L. E.; Al-Saffar, N. M.; Workman, P.; Leach, M. O.; Ronen, S. M. *Cancer Res.* **2005**, *65*, 3356.
(187) Ross, J.; Najjar, A. M.; Sankaranarayanapillai, M.; Tong, W. P.; Kaluarachchi, K.; Ronen, S. M. *Mol. Cancer Ther.* **2008**, *7*, 2556.
(188) Klawitter, J.; Anderson, N.; Klawitter, J.; Christians, U.; Leibfritz, D.; Eckhardt, S. G.; Serkova, N. J. *Br. J. Cancer* **2009**, *100*, 923.
(189) Sankaranarayanapillai, M.; Tong, W. P.; Yuan, Q.; Bankson, J. A.; Dafni, H.; Bornmann, W. G.; Soghomonyan, S.; Pal, A.; Ramirez, M. S.; Webb, D.; Kaluarachchi, K.; Gelovani, J. G.; Ronen, S. M. *Mol. Imaging* **2008**, *7*, 92.
(190) Al-Saffar, N. M.; Troy, H.; Ramirez de Molina, A.; Jackson, L. E.; Madhu, B.; Griffiths, J. R.; Leach, M. O.; Workman, P.; Lacal, J. C.; Judson, I. R.; Chung, Y. L. *Cancer Res.* **2006**, *66*, 427.
(191) Krishnamachary, B.; Glunde, K.; Wildes, F.; Mori, N.; Takagi, T.; Raman, V.; Bhujwalla, Z. M. *Cancer Res.* **2009**, *69*, 3464.
(192) Campos, J. M.; Nunez, M. C.; Sanchez, R. M.; Gomez-Vidal, J. A.; Rodriguez-Gonzalez, A.; Banez, M.; Gallo, M. A.; Lacal, J. C.; Espinosa, A. *Bioorg. Med. Chem.* **2002**, *10*, 2215.
(193) Lacal, J. C. *IDrugs* **2001**, *4*, 419.
(194) Meister, G.; Tuschl, T. *Nature* **2004**, *431*, 343.
(195) Fire, A.; Xu, S.; Montgomery, M. K.; Kostas, S. A.; Driver, S. E.; Mello, C. C. *Nature* **1998**, *391*, 806.
(196) Gallagher, F. A.; Kettunen, M. I.; Hu, D. E.; Jensen, P. R.; Zandt, R. I.; Karlsson, M.; Gisselsson, A.; Nelson, S. K.; Witney, T. H.; Bohndiek, S. E.; Hansson, G.; Peitersen, T.; Lerche, M. H.; Brindle, K. M. *Proc. Natl. Acad. Sci. U.S.A.* **2009**, *106*, 19801.
(197) Artemov, D.; Solaiyappan, M.; Bhujwalla, Z. M. *Cancer Res.* **2001**, *61*, 3039.
(198) Kato, Y.; Holm, D. A.; Okollie, B.; Artemov, D. *Neuro-Oncology* **2010**, *12*, 71.
(199) Wolf, W.; Presant, C. A.; Waluch, V. *Adv. Drug Delivery Rev.* **2000**, *41*, 55.
(200) van Laarhoven, H. W.; Klomp, D. W.; Rijpkema, M.; Kamm, Y. L.; Wagener, D. J.; Barentsz, J. O.; Punt, C. J.; Heerschap, A. *NMR Biomed.* **2007**, *20*, 128.
(201) Li, C.; Penet, M. F.; Winnard, P., Jr.; Artemov, D.; Bhujwalla, Z. M. *Clin. Cancer Res.* **2008**, *14*, 515.
(202) Reid, D. G.; Murphy, P. S. *Drug Discovery Today* **2008**, *13*, 473.
(203) Yu, J.-X.; Cui, W.; Zhao, D.; Mason, R. P. In *Fluorine and Health*; Tressaud, A., Haufe, G., Eds.; Elsevier B.V.: Amsterdam, 2008.
(204) Kato, Y.; Okollie, B.; Artemov, D. *Magn. Reson. Med.* **2006**, *55*, 755.
(205) Griffiths, J. R.; Glickson, J. D. *Adv. Drug Delivery Rev.* **2000**, *41*, 75.
(206) O'Reilly, S. M.; Newlands, E. S.; Glaser, M. G.; Brampton, M.; Rice-Edwards, J. M.; Illingworth, R. D.; Richards, P. G.; Kennard, C.; Colquhoun, I. R.; Lewis, P.; et al. *Eur. J. Cancer* **1993**, *29A*, 940.
(207) Gillies, R. J.; Raghunand, N.; Garcia-Martin, M. L.; Gatenby, R. A. *IEEE Eng. Med. Biol. Mag.* **2004**, *23*, 57.

CR9004007